A General Solution of the Ripple-Averaged Kinetic Equation (GSRAKE)

C.D. Beidler, W.D. D'haeseleer

IPP 2/327 October 1994

MAX-PLANCK-INSTITUT FÜR PLASMAPHYSIK

85748 GARCHING BEI MÜNCHEN

MAX-PLANCK-INSTITUT FÜR PLASMAPHYSIK

GARCHING BEI MÜNCHEN

A General Solution of the Ripple-Averaged Kinetic Equation (GSRAKE)

C.D. BEIDLER, W.D. D'HAESELEER

IPP 2/327 October 1994

Die nachstehende Arbeit wurde im Rahmen des Vertrages zwischen dem Max-Planck-Institut für Plasmaphysik und der Europäischen Atomgemeinschaft über die Zusammenarbeit auf dem Gebiete der Plasmaphysik durchgeführt.

A GENERAL SOLUTION
OF THE
RIPPLE-AVERAGED KINETIC EQUATION
(GSRAKE)

C.D. Beidler
Max-Planck-Institut für Plasmaphysik
IPP–EURATOM Association
D-85748 Garching bei München, Germany

W.D. D'haeseleer
The NET Team
c/o Max-Planck-Institut für Plasmaphysik
D-85748 Garching bei München, Germany

ABSTRACT

A General Solution of the Ripple-Averaged Kinetic Equation, GSRAKE, is presented and used to investigate neoclassical transport in the model magnetic field of a simple stellarator. No assumptions are made as to the relative sizes of the collision frequency, ν, and poloidal precessional frequency, Ω_θ, so that the solution is valid throughout the entire *long-mean-free-path* regime. Separate but fully self-consistent treatments of both localized and non-localized particles are provided; the interaction between these two classes of particles is accounted for through a set of appropriate physical boundary conditions. All drift terms present within the framework of the ripple-averaged theory are included; in particular, for localized particles $\Omega_\theta = \Omega_E + \Omega_{\nabla B}$ is comprised of both the $\mathbf{E}\times\mathbf{B}$ and ∇B precessional frequencies. The solution is thus equally valid in the $\Omega_E \gg \Omega_{\nabla B}$ and the $\Omega_E = 0$ limits of standard neoclassical theory. A detailed comparion of results with those of the FLOCS code (D'haeseleer, Hitchon and Shohet, 1991 J. Comput. Phys. 95, 117) is undertaken; estimates of neoclassical transport coefficients obtained from several codes are also presented. Good agreement of results is found in all of these comparisons, GSRAKE requiring but a tiny fraction of the computational time necessary for the other codes.

I. INTRODUCTION

Theoretical efforts to understand and describe neoclassical transport in toroidal stellarators have been undertaken now for more than two decades. During this period of time, a number of approaches, both analytical and numerical, have been developed to investigate various aspects of this topic. Most of the early literature (which served to define the subject) is analytic in nature [1-4] and many subsequent authors [5-12] have also chosen this approach to further refine, develop and extend the initial theories. Analytic descriptions of neoclassical transport are attractive since they provide physical insight into the various transport mechanisms and offer quick estimates of the associated neoclassical losses. They have the drawback, however, of employing a number of simplifying assumptions; these make the given problem tractable at the expense of limiting the validity of the results obtained. The appearance and current prevalence of numerical methods for the determination of neoclassical transport coefficients in stellarators has been driven to a large extent by the desire to avoid many of these assumptions. Among these numerical calculations are a number of Monte Carlo simulations [13-18], two solutions of the bounce-averaged Fokker-Planck equation, FPSTEL [19] and FLOCS [20], and a solution of the drift-kinetic equation, DKES [21,22]. The principal disadvantage of these computational approaches lies in the significant amounts of computer time which they consume. (Note: the list of references cited above is meant to be a representative sample from the extensive literature and is by no means exhaustive.)

The paper at hand is devoted to a general solution of the ripple-averaged kinetic equation (henceforth referred to by its acronym, GSRAKE) and to some initial examples of its use in the study of neoclassical transport in stellarators. The claim of a "general" solution rests on three important properties which are summarized in the following.

- The solution is valid throughout the entire *long-mean-free-path* (*lmfp*) regime, i.e., at all values of collision frequency for which the ripple-averaged kinetic equation is appropriate.
- The solution encompasses all of pitch-angle space. It is common practice in stellarator theory to divide velocity space into two regions, one in which *localized* particles exist (trapped in the stellarator's helical ripple) and a second where the particles are *non-localized* (either on completely passing trajectories or executing tokamak-banana-like orbits). Both regions are considered on an equal footing in GSRAKE, and their interaction is also accounted for.

• All drift terms present within the framework of the ripple-averaged theory have been included. In particular, the poloidal rotation of localized particles includes contributions due to the $\mathbf{E}\times\mathbf{B}$ and ∇B drifts, designated Ω_E and $\Omega_{\nabla B}$, respectively. The common assumption $\Omega_E \gg \Omega_{\nabla B}$ may thus be dropped; indeed, GSRAKE makes it possible to consider cases where precisely the opposite is true.

Many of these properties can also be claimed by the other numerical calculations mentioned above. GSRAKE has the additional distinction, however, of great computational speed; CPU times of a few seconds or less are typical even when the collision frequency becomes very small. Its speed and general nature combine to set GSRAKE apart from previous analytical and numerical approaches and make it particularly well-suited for neoclassical transport studies.

This paper is organized in the following manner. The ripple-averaged kinetic equations for localized and non-localized particles are introduced in Section II. An idealized model magnetic field has been assumed (although more general expressions for B are also possible) to simplify the presentation and to facilitate an interpretation of the results given in later sections. The solution of these kinetic equations using a numerical scheme is described in Section III. As this scheme combines several standard numerical techniques, only the GSRAKE-specific implementation thereof will be detailed. Section IV is devoted to a brief description of the FLOCS code, in preparation for the detailed comparison of GSRAKE and FLOCS results which follows in Section V. Monte Carlo and DKES estimates of neoclassical transport coefficients are also presented in this section and compared with the predictions of GSRAKE and FLOCS. Some final comments and a summary of the results are provided in Section VI.

II. THE RIPPLE-AVERAGED KINETIC EQUATION

— (a) Preliminaries

Consider the simple model for the magnitude of the magnetic field in a toroidal stellarator

$$B/B_0 = 1 - \epsilon(r)\cos\theta - \epsilon_h(r)\cos(\ell\theta - p\phi) \tag{1}$$

expressed in the magnetic coordinate system (r,ϕ,θ) [14]. Here r is a flux surface label (related to the toroidal flux through the expression $\psi = B_0 r^2/2$), ϕ and θ are toroidal and poloidal angle-like variables, respectively, ℓ is the field multipolarity and p is the field period number. The magnitude of the toroidal modulation of B is given by ϵ (not

necessarily equal to $\epsilon_t = r/R_0$, the inverse aspect ratio); ϵ_h is the magnitude of the stellarator's helical ripple. It is explicitly assumed that $\epsilon,\epsilon_h \ll 1$.

Field lines are "straight" in the given coordinate system, specified through the equation $\theta = \theta_0 + \iota(r)\phi$, where ι is the rotational transform. Typically for stellarators $\iota \ll |\ell\iota - p|$; along magnetic field lines, B is thus characterized by a rapid modulation due to the helical ripple superimposed over a slower toroidal modulation. Stated somewhat differently, θ remains nearly constant over one period of the helical ripple phase $\eta \equiv \ell\theta - p\phi$.

To complete the specification of phase space it is common practice to choose the total energy, $\mathcal{E} = \kappa + q\Phi(r)$, and the magnetic moment, $\mu = mv_\perp^2/2B$, as velocity-space variables since these quantities are adiabatic invariants within the framework of guiding-center theory. Here $\kappa = mv^2/2$ is the kinetic energy with $v^2 = v_\parallel^2 + v_\perp^2$, Φ is the electrostatic potential and m and q are the particle mass and charge, respectively. For the set of variables $(r,\phi,\theta,\mathcal{E},\mu)$ and the model magnetic field of equation (1), the time-independent drift kinetic equation may then be expressed

$$\frac{dr}{dt}\frac{\partial F}{\partial r} + \frac{d\phi}{dt}\frac{\partial F}{\partial \phi} + \frac{d\theta}{dt}\frac{\partial F}{\partial \theta} = \mathcal{L}_\mu(F) \tag{2}$$

where the drift equations are given by

$$\frac{dr}{dt} = \frac{v_d}{\epsilon_t}(1+\lambda^2)\frac{B_0}{B}\left(\epsilon\sin\theta + \ell\epsilon_h\sin\eta\right),$$

$$\frac{d\phi}{dt} = \frac{v_\parallel}{R},$$

$$\frac{d\theta}{dt} = \frac{\iota v_\parallel}{R} - \frac{1}{rB_0}\frac{\partial\Phi}{\partial r} + \frac{v_d}{\epsilon_t}(1+\lambda^2)\frac{B_0}{B}\left(\frac{\partial\epsilon}{\partial r}\cos\theta + \frac{\partial\epsilon_h}{\partial r}\cos\eta\right),$$

with

$$v_d = \frac{\kappa}{qB_0R_0}, \qquad \lambda = \frac{v_\parallel}{v}, \qquad R = R_0 + r\cos\theta,$$

and with collisional processes modeled using the Lorentz collision operator

$$\mathcal{L}_\mu(F) = \nu\frac{2\kappa}{B}\lambda\frac{\partial}{\partial\mu}\left(\mu\lambda\frac{\partial F}{\partial\mu}\right),$$

where ν is the 90-degree deflection frequency. The $F = F(r,\phi,\theta,\mathcal{E},\mu)$ appearing in equation (2) is the total distribution function — to this point no ordering assumptions have been made.

The individual terms appearing in the drift equations are identified with: (a) rapid particle motion along the magnetic field with velocity $v_\parallel$; and (b) the much slower motion perpendicular to $\mathbf{B}$ with characteristic velocities v_d and $(-\partial\Phi/\partial r)/B_0$, arising due to the ∇B and $\mathbf{E}\times\mathbf{B}$ drifts, respectively. The magnitude of the parallel velocity may be determined from

$$u \equiv |v_\parallel| = \left(\frac{2}{m}(\kappa - \mu B)\right)^{1/2} = \left(\frac{4\mu B_0 \epsilon_h}{m}\right)^{1/2} \left(k^2 - \sin^2(\eta/2)\right)^{1/2},$$

where

$$k^2 = \frac{\kappa/\mu B_0 - 1 + \epsilon\cos\theta + \epsilon_h}{2\epsilon_h}.$$

Although it is not a constant of the motion, the use of k^2 as pitch-angle variable in place of μ does offer certain advantages if the toroidicity of B may be considered as a negligible perturbation to the sinusoidal symmetry of a helical ripple well (which is usually expressed as the requirement that $\alpha \equiv \epsilon\iota/(\epsilon_h|\ell\iota - p|) \ll 1$). In this case only localized particles can undergo reflection in the magnetic field ($u = 0$) and must therefore satisfy $0 \le k^2 \le 1$, whereas non-localized particles are considered to be *locally passing* and thus characterized by $k^2 > 1$. Clearly then, the boundary in pitch-angle space separating localized from non-localized particles occurs at $k^2 = 1$.

The time required by localized particles to execute a complete "bounce" in the helical ripple may now be determined from

$$\tau_b = \oint \frac{dl}{v_\parallel}$$

where $dl = R\,d\phi = R\,d\eta/(\ell\iota - p)$ is taken along a field line. Explicitly, the bounce time becomes

$$\tau_b = \frac{2R}{|\ell\iota - p|}\int_{-\eta_b}^{\eta_b}\frac{d\eta}{u} = \frac{4R}{|\ell\iota - p|}\left(\frac{m}{\mu B_0 \epsilon_h}\right)^{1/2} K(k)$$

where $\eta_b = 2\sin^{-1}k$ and $K(k)$ is the complete elliptic integral of the first kind. Similarly, the time required for a non-localized particle to "traverse" the helical ripple is

$$\tau_t = \frac{R}{|\ell\iota - p|}\int_{-\pi}^{\pi}\frac{d\eta}{u} = \frac{2R}{|\ell\iota - p|}\left(\frac{m}{\mu B_0 \epsilon_h}\right)^{1/2} \frac{K(1/k)}{k}.$$

— *(b) Ripple-Localized Particles*

Localized particles are said to be in the *long-mean-free-path* (*lmfp*) regime if the condition $\tau_b \nu_{eff} \ll 1$ is satisfied, where $\nu_{eff} \equiv \nu/2\epsilon_h$ is the frequency with which particles are collisionally removed from the helical ripple. Such particles thus have a chance to complete several bounces and it becomes physically meaningful to consider averaging over this (nearly) periodic motion. Before doing so, however, k^2 is explicitly chosen as the pitch-angle variable for ripple-localized particles in place of μ and equation (2) is rewritten as

$$\frac{dr}{dt}\frac{\partial F}{\partial r} + \frac{d\phi}{dt}\frac{\partial F}{\partial \phi} + \frac{d\theta}{dt}\frac{\partial F}{\partial \theta} + \frac{dk^2}{dt}\frac{\partial F}{\partial k^2} = \mathcal{L}_{k^2}(F).$$

The time rate of change of k^2 appearing in this equation may be determined from

$$\frac{dk^2}{dt} = \frac{\partial k^2}{\partial r}\frac{dr}{dt} + \frac{\partial k^2}{\partial \theta}\frac{d\theta}{dt}$$

where the partial derivatives are taken at constant $\mathcal{E}$ and μ. The Lorentz collision operator expressed in terms of k^2 has the form

$$\mathcal{L}_{k^2}(F) = \nu_{eff}\left(\frac{\kappa}{\mu B_0}\right)^2 \frac{B_0}{B}\frac{\lambda}{\epsilon_h}\frac{\partial}{\partial k^2}\left(\frac{\kappa}{\mu B_0}\lambda\frac{\partial F}{\partial k^2}\right).$$

This kinetic equation may now be time averaged over the periodic bounce motion of particles localized in the helical ripple using the operator

$$\langle x\rangle_r = \frac{1}{\tau_b}\oint dl\,\frac{x}{v_\parallel},$$

which has been chosen so as to annihilate the term $(d\phi/dt)(\partial F/\partial\phi)$. Simultaneously, the kinetic equation will be linearized; i.e., it is assumed that the distribution function for ripple-localized particles may be written $F = F_m + f_r$, where F_m is a local Maxwellian and f_r the small perturbation therefrom. For toroidal stellarators in the *lmfp* regime the variation of f_r about its average value is small over the course of a single ripple [23] — the dominant neoclassical transport mechanisms are adequately described if f_r is taken to be constant over this scale length. The averaging procedure is then straightforward and the result is referred to as the ripple-averaged kinetic equation for localized particles

$$\langle \dot{r}\rangle_r \frac{\partial F_m}{\partial r} + \langle \dot{\theta}\rangle_r \frac{\partial f_r}{\partial \theta} + \langle \dot{k}^2\rangle_r \frac{\partial f_r}{\partial k^2} = \langle \mathcal{L}_{k^2}(f_r)\rangle_r, \tag{3}$$

where

$$\langle \dot{r} \rangle_r = v_d \frac{\epsilon}{\epsilon_t} \sin\theta \Big(1 + \langle \lambda^2 \rangle_r \Big),$$

$$\langle \dot{\theta} \rangle_r = \Omega_E + \Omega_h \Big(\langle \cos\eta \rangle_r + \langle \lambda^2 \cos\eta \rangle_r \Big) + \Omega_t \cos\theta \Big(1 + \langle \lambda^2 \rangle_r \Big),$$

$$\langle \dot{k}^2 \rangle_r = \Omega_E \, \epsilon \sin\theta \, \frac{A(k^2)}{A'(k^2)} - \Omega_h \, \frac{\epsilon}{2\epsilon_h} \sin\theta \left(\frac{A(k^2)}{A'(k^2)} + \frac{\kappa}{\mu B_0} \frac{\langle \lambda^4 \rangle_r}{\epsilon_h} \right),$$

$$\langle \mathcal{L}_{k^2}(f_r) \rangle_r = \nu_{eff} \left(\frac{\kappa}{\mu B_0} \right)^2 \left(\Big(1 + \langle \lambda^2 \rangle_r \Big) \frac{\partial f_r}{\partial k^2} + \frac{A(k^2)}{A'(k^2)} \frac{\partial^2 f_r}{(\partial k^2)^2} \right),$$

with a dot denoting d/dt and with

$$\Omega_E = \frac{-1}{rB_0} \frac{\partial \Phi}{\partial r}, \qquad \Omega_h = \frac{v_d}{\epsilon_t} \frac{\partial \epsilon_h}{\partial r}, \qquad \Omega_t = \frac{v_d}{\epsilon_t} \frac{\partial \epsilon}{\partial r},$$

$$\langle \lambda^2 \rangle_r = \epsilon_h \frac{\mu B_0}{\kappa} \frac{A(k^2)}{A'(k^2)},$$

$$\langle \cos\eta \rangle_r = 1 - 2k^2 + \frac{A(k^2)}{A'(k^2)},$$

$$\langle \lambda^4 \rangle_r = \frac{4}{3} \left(\epsilon_h \frac{\mu B_0}{\kappa} \right)^2 \left((2k^2 - 1) \frac{A(k^2)}{A'(k^2)} + k^2(1 - k^2) \right),$$

$$\langle \lambda^2 \cos\eta \rangle_r = (1 - 2k^2) \langle \lambda^2 \rangle_r + \frac{\kappa}{\mu B_0} \frac{\langle \lambda^4 \rangle_r}{\epsilon_h},$$

$$A(k^2) = 8 \Big(E(k) - (1 - k^2) K(k) \Big), \qquad A'(k^2) = \frac{\partial A(k^2)}{\partial k^2} = 4K(k),$$

where $K(k)$ and $E(k)$ are complete elliptic integrals of the first and second kinds, respectively. It is also common in the literature to refer to equation (3) as the *bounce-averaged* kinetic equation. The reader's attention is directed to the following points.

- The averaging procedure yields $\langle v_\parallel \rangle_r = 0$, thereby eliminating the rapid motion along $\mathbf{B}$ from the description of localized particles. Odd functions of η also vanish (e.g., $\langle \sin\eta \rangle_r = 0$).
- While carrying out the averages it may be assumed that $B_0/B = 1$. Corrections to this assumption are $\mathcal{O}(\epsilon, \epsilon_h)$ and may therefore be neglected.

• Terms in the ripple-averaged drift equations which contain $\langle\lambda^2\rangle_r$ and/or $\langle\lambda^4\rangle_r/\epsilon_h$ are also $\mathcal{O}(\epsilon_h)$ and are likewise usually ignored. They have been retained here because they have counterparts in the drift equations for non-localized particles which are non-negligible (as will be shown below); this assures continuity of these terms at the $k^2 = 1$ boundary.

• In stellarators, the ambipolarity constraint on the particle fluxes generally yields a potential for which $q\Phi/\epsilon T$ is $\mathcal{O}(1)$, ϵT being the kinetic energy of thermal particles. It then follows that $\epsilon_h\Omega_E/\Omega_h$ is $\mathcal{O}(1)$ for thermal particles as well, i.e., the two terms appearing in $\langle\dot{k}^2\rangle_r$ are similar in magnitude. This is mentioned here because the term containing Ω_E has been overlooked in the previous calculations [19,20].

— (c) Non-Localized Particles

The ripple average introduced in the preceeding sub-section is performed over the periodic bounce motion of localized particles. Such a procedure is clearly impossible in the case of non-localized particles; instead the kinetic equation is averaged over the time required by non-localized particles to traverse a single helical-ripple well. This process results in two kinetic equations, one for particles with parallel velocity in the *forward* direction ($u/v_{\|} = 1$) and the other for particles moving in the *backward* direction ($u/v_{\|} = -1$). In either case, the ripple average is defined as

$$\langle x\rangle = \frac{1}{\tau_t}\int_{-\pi}^{\pi}\frac{R\,d\eta}{|\ell_t - p|}\,\frac{x}{u}\,.$$

Once again, k^2 will be used as pitch-angle variable instead of μ, although for numerical purposes it will prove more convenient to employ its reciprocal, $\zeta^2 \equiv 1/k^2$. The time rate of change of ζ^2 is given by

$$\frac{d\zeta^2}{dt} = \frac{\partial\zeta^2}{\partial r}\frac{dr}{dt} + \frac{\partial\zeta^2}{\partial\theta}\frac{d\theta}{dt} = -(\zeta^2)^2\,\frac{dk^2}{dt}\,,$$

and the collision operator becomes

$$\mathcal{L}_{\zeta^2}(F) = \nu_{eff}\left(\frac{\zeta^2\kappa}{\mu B_0}\right)^2\frac{B_0}{B}\frac{\lambda}{\epsilon_h}\frac{\partial}{\partial\zeta^2}\left(\zeta^2\,\frac{\zeta^2\kappa}{\mu B_0}\,\lambda\,\frac{\partial F}{\partial\zeta^2}\right).$$

Again coupling the averaging procedure with the linearization of the distribution function about a local Maxwellian, one obtains the ripple-averaged kinetic equation for non-localized particles traveling in the forward direction

$$\langle \dot{r} \rangle \frac{\partial F_m}{\partial r} + \langle \dot{\theta} \rangle_f \frac{\partial f_f}{\partial \theta} + \langle \dot{\zeta}^2 \rangle_f \frac{\partial f_f}{\partial \zeta^2} = \langle \mathcal{L}_{\zeta^2}(f_f) \rangle \,, \tag{4}$$

where

$$\langle \dot{r} \rangle = v_d \frac{\epsilon}{\epsilon_t} \sin\theta \left(1 + \langle \lambda^2 \rangle\right),$$

$$\langle \dot{\theta} \rangle_f = \frac{\not{\epsilon} \langle u \rangle}{R} + \Omega_E + \Omega_h \Big(\langle \cos\eta \rangle + \langle \lambda^2 \cos\eta \rangle \Big) + \Omega_t \cos\theta \left(1 + \langle \lambda^2 \rangle\right),$$

$$\langle \dot{\zeta}^2 \rangle_f = (\zeta^2)^2 \frac{\epsilon}{2\epsilon_h} \sin\theta \frac{\not{\epsilon} \langle u \rangle}{R} - \zeta^2 \Omega_E \, \epsilon \sin\theta \frac{2E(\zeta)}{K(\zeta)} + \zeta^2 \Omega_h \frac{\epsilon}{2\epsilon_h} \sin\theta \left(\frac{2E(\zeta)}{K(\zeta)} + \frac{\zeta^2 \kappa}{\mu B_0} \frac{\langle \lambda^4 \rangle}{\epsilon_h} \right),$$

$$\langle \mathcal{L}_{\zeta^2}(f_f) \rangle = -\nu_{eff} \left(\frac{\zeta^2 \kappa}{\mu B_0} \right)^2 \left(\left(1 + \langle \lambda^2 \rangle - \frac{4E(\zeta)}{K(\zeta)} \right) \frac{\partial f_f}{\partial \zeta^2} - \zeta^2 \frac{2E(\zeta)}{K(\zeta)} \frac{\partial^2 f_f}{(\partial \zeta^2)^2} \right),$$

with

$$\langle u \rangle = v \left(2\epsilon_h \frac{\mu B_0}{\zeta^2 \kappa} \right)^{1/2} \frac{\pi}{2K(\zeta)},$$

$$\langle \lambda^2 \rangle = \epsilon_h \frac{\mu B_0}{\zeta^2 \kappa} \frac{2E(\zeta)}{K(\zeta)},$$

$$\langle \cos\eta \rangle = 1 - \frac{2}{\zeta^2} + \frac{2E(\zeta)}{\zeta^2 K(\zeta)},$$

$$\langle \lambda^4 \rangle = \frac{4}{3} \left(\epsilon_h \frac{\mu B_0}{\zeta^2 \kappa} \right)^2 \left((2 - \zeta^2) \frac{2E(\zeta)}{K(\zeta)} + \zeta^2 - 1 \right),$$

$$\langle \lambda^2 \cos\eta \rangle = \left(1 - \frac{2}{\zeta^2} \right) \langle \lambda^2 \rangle + \frac{\kappa}{\mu B_0} \frac{\langle \lambda^4 \rangle}{\epsilon_h}.$$

In the same manner, the ripple-averaged kinetic equation for non-localized particles with parallel velocity directed backwards is given by

$$\langle \dot{r} \rangle \frac{\partial F_m}{\partial r} + \langle \dot{\theta} \rangle_b \frac{\partial f_b}{\partial \theta} + \langle \dot{\zeta}^2 \rangle_b \frac{\partial f_b}{\partial \zeta^2} = \langle \mathcal{L}_{\zeta^2}(f_b) \rangle \,, \tag{5}$$

where the expressions for $\langle \dot{\theta} \rangle_b$ and $\langle \dot{\zeta}^2 \rangle_b$ are identical to those of $\langle \dot{\theta} \rangle_f$ and $\langle \dot{\zeta}^2 \rangle_f$ with the exception that $\langle u \rangle$ must be replaced with $-\langle u \rangle$. Otherwise, in all the preceeding expressions, the lack of an f or b subscript on a ripple-averaged quantity indicates that that quantity is identical in both the forward and backward kinetic equations.

As in the previous case for localized particles, ripple averaging has eliminated quantities which are odd functions of η. On the other hand, the parallel motion along $\mathbf{B}$ (with averaged velocity $\langle u \rangle$) of non-localized particles remains and is responsible for the dominant contribution to $\langle \dot{\theta} \rangle_{f,b}$ and $\langle \dot{\zeta}^2 \rangle_{f,b}$. It is also to be expected that terms containing $\langle \lambda^2 \rangle$ and $\langle \lambda^4 \rangle$ are of more importance in the drift equations for non-localized particles and, indeed, using the definition of k^2 to obtain the expression

$$\frac{\zeta^2 \kappa}{\mu B_0} \approx \zeta^2 + \epsilon_h (2 - \zeta^2),$$

together with small-argument approximations for the complete elliptic integrals, $K(\zeta) \approx (\pi/2)(1 + \zeta^2/4)$ and $E(\zeta) \approx (\pi/2)(1 - \zeta^2/4)$, one finds that near $\zeta^2 = 0$, $\langle \lambda^2 \rangle$ and $\langle \lambda^4 \rangle$ are both $\mathcal{O}(1)$.

III. THE METHOD OF SOLUTION

The solution of the ripple-averaged kinetic equations (3)–(5) is undertaken using common numerical techniques, so that its description here may be confined to several specific points. First, the θ dependence of f is expressed in Fourier series,

$$\begin{pmatrix} f_r \\ f_f \\ f_b \end{pmatrix} = \frac{\partial F_m}{\partial r} \left\{ \sum_{m=0}^{\infty} \begin{pmatrix} C_r^{(m)}(k^2) \\ C_f^{(m)}(\zeta^2) \\ C_b^{(m)}(\zeta^2) \end{pmatrix} \cos m\theta + \sum_{m=1}^{\infty} \begin{pmatrix} S_r^{(m)}(k^2) \\ S_f^{(m)}(\zeta^2) \\ S_b^{(m)}(\zeta^2) \end{pmatrix} \sin m\theta \right\} \tag{6}$$

being assumed for the ripple-localized, forward and backward distribution functions, respectively. In practice, the infinite series must be truncated at an appropriate value of m_{max}, yielding a system in which three sets of $2m_{max} + 1$ coupled ordinary differential equations are to be solved simultaneously. It is to be hoped, of course, that a small number of Fourier harmonics is sufficient to accurately describe the perturbed distribution function (this hope is put to the test in Section V by investigating the convergence properties of the solution with increasing m_{max}).

Solutions for the unknown Fourier coefficients are to be sought using discrete (finite difference) techniques. It is therefore necessary to represent the solution domain by a finite number of k^2 and ζ^2 values (designated k_i^2 and ζ_j^2, respectively, where $i = 1, 2, 3, \ldots, n_k$ and $j = 1, 2, 3, \ldots, n_\zeta$), referred to as nodes. The spacing between nodes is allowed to be non-uniform; this is useful at small values of ν where solutions tend to be localized about $k^2 = 1$, allowing one to increase the density of nodes in this region while leaving the remainder of the domain more sparsely populated. For the sake of simplicity, the choosing of nodes is done so as to be appropriate in each

of the three solution regions (localized, forward and backward), i.e., $n_k = n_\zeta = n$, $k_i^2 = \zeta_i^2$ for $i = 1, 2, 3, \ldots, n$, where the value of n is determined by the particulars of the given problem. Regardless of the value of n, the nodes are always chosen so that $k_{i+1}^2 > k_i^2$ ($\zeta_{i+1}^2 > \zeta_i^2$) with $k_1^2 = \zeta_1^2 = 0$ and $k_n^2 = \zeta_n^2 = 1$. Furthermore, the spacing of nodes satisfies $\delta_{i+1} \leq \delta_i \leq \delta_{max}$, where $\delta_i = k_{i+1}^2 - k_i^2 = \zeta_{i+1}^2 - \zeta_i^2$ and δ_{max} is the maximum spacing allowed (for all results presented here $\delta_{max} = 0.04$, i.e., the limiting case for sufficiently large values of ν is given by $k_i^2 = \zeta_i^2 = (i-1)\delta_{max}$ with $n = 26$). Differentiation is carried out using the discrete approximations of the finite difference formulae (second-order accuracy)

$$\left.\frac{\partial f}{\partial x}\right|_{x=x_i} = d_{i+1} f_{i+1} - (d_{i+1} + d_{i-1}) f_i + d_{i-1} f_{i-1}$$

$$i = 2, 3, 4, \ldots, n-1$$

$$\left.\frac{\partial^2 f}{\partial x^2}\right|_{x=x_i} = g_{i+1} f_{i+1} - (g_{i+1} + g_{i-1}) f_i + g_{i-1} f_{i-1}$$

with $f_i = f(x_i)$ and where

$$d_{i+1} = \frac{\delta_{i-1}}{\delta_i(\delta_i + \delta_{i-1})}, \qquad d_{i-1} = \frac{-\delta_i}{\delta_{i-1}(\delta_i + \delta_{i-1})},$$

$$g_{i+1} = \frac{2d_{i+1}}{\delta_i} - 2d_{i+1}(d_{i+1} + d_{i-1}), \qquad g_{i-1} = \frac{-2d_{i-1}}{\delta_{i-1}} - 2d_{i-1}(d_{i+1} + d_{i-1}),$$

where one must substitute $f = f_r$, $x = k^2$ or $f = f_{f,b}$, $x = \zeta^2$ as appropriate. It is easy to verify that these formulae reduce to the usual expressions for central differences when $\delta_i = \delta_{i-1}$.

For the $i = 1$ nodes, forward differencing is employed. Here, far from $k^2 = 1$, the node spacing is always uniform and given by δ_{max} so that one has

$$\left.\frac{\partial f}{\partial x}\right|_{x=0} = \frac{-3f_1 + 4f_2 - f_3}{2\delta_{max}}.$$

No expression for $\partial^2 f/\partial x^2$ is necessary since the term multiplying the second derivative vanishes at both $k^2 = 0$ and $\zeta^2 = 0$.

The physical requirement that the distribution function as well as its derivative with respect to the pitch-angle variable be continuous at $k^2 = 1$ leads to the following set of boundary conditions at the $i = n$ nodes,

$$f_r(k^2=1) = f_f(k^2=1),$$

$$f_f(k^2=1) = f_b(k^2=1),$$

$$2\frac{\partial f_r}{\partial k^2}\bigg|_{k^2=1} + \frac{\partial f_f}{\partial \zeta^2}\bigg|_{k^2=1} + \frac{\partial f_b}{\partial \zeta^2}\bigg|_{k^2=1} = 0,$$

where differentiation at $k^2 = 1$ is performed using the backward-differencing formula

$$\frac{\partial f}{\partial x}\bigg|_{x=1} = \frac{\delta_{n-1}}{\delta_{n-2}(\delta_{n-1}+\delta_{n-2})} f_{n-2} - \frac{(\delta_{n-1}+\delta_{n-2})}{\delta_{n-1}\,\delta_{n-2}} f_{n-1} + \frac{(2\delta_{n-1}+\delta_{n-2})}{\delta_{n-1}(\delta_{n-1}+\delta_{n-2})} f_n.$$

These boundary conditions determine the solution for the perturbed distribution function to within a constant, independent of both θ and k^2. This constant is ascertained from the additional requirement

$$\int dV_r\, f_r + \int dV_f\, f_f + \int dV_b\, f_b = 0, \tag{7}$$

where the differential volume elements are given by $dV_r = J_r\, dr\, d\theta\, d\kappa\, dk^2$ and $dV_{f,b} = J_{f,b}\, dr\, d\theta\, d\kappa\, d\zeta^2$, and

$$J_r = 16\pi r R \left(\frac{\mu B_0}{\kappa}\right)^{3/2} \frac{\kappa^{1/2}\epsilon_h^{1/2}}{m^{3/2}} K(k),$$

$$J_f = J_b = 8\pi r R \left(\frac{\mu B_0}{\zeta^2 \kappa}\right)^{3/2} \frac{\kappa^{1/2}\epsilon_h^{1/2}}{m^{3/2}} K(\zeta)$$

are the appropriate ripple-averaged Jacobians. This requirement is equivalent to the conservation of the total number of particles enforced by the FLOCS code at each step in its time-evolution scheme (a point clarified further in the following section). Given the Fourier ansatz of equation (6) for the perturbed distribution function, equation (7) may also be written

$$\int_0^1 dk^2\, J_r C_r^{(0)} + \int_0^1 d\zeta^2\, (J_f C_f^{(0)} + J_b C_b^{(0)}) = 0.$$

As input, GSRAKE requires a description of the model magnetic field (e.g., R_0, B_0, ι, ϵ, ϵ_h, $\partial\epsilon/\partial r$, $\partial\epsilon_h/\partial r$) and plasma parameters (e.g., T, Ω_E, ν). With this information, an appropriate number and spacing of nodes is chosen. The value of m_{max} is also an input, limited only by the available computer memory. GSRAKE generates automatically the equations for each Fourier harmonic $\cos m\theta$ and $\sin m\theta$ ($m = 0, 1, \ldots, m_{max}$) in each of the three solution regions, using the finite difference formulae and boundary conditions described above. A system of N equations in N unknowns results — where $N = 3n(2m_{max} + 1)$ — which is solved by Gaussian elimination. This procedure is straightforward but for a single exception. Although in principle it is possible to determine the solution constant using equation (7) after matrix inversion, numerical stability is insured only if this equation is explicitly included as one of the original N; it replaces the third boundary condition in the $m = 0$ set of equations.

IV. A BRIEF OVERVIEW OF FLOCS

The FLOCS code solves essentially the same set of averaged kinetic equations as GSRAKE, so that a comparison of results from the two codes is a logical undertaking. FLOCS has been described thoroughly elsewhere [20], but a short overview is necessary here to point out similarities and differences in the two codes.

FLOCS solves the *time-dependent* ripple-averaged kinetic equation by central differencing (second-order accuracy) on a 2D mesh (θ, k^2) using an explicit time-relaxation scheme. The variable k^2 is used for both localized and non-localized particles; a multi-mesh approach (each mesh with successively coarser spacing in k^2) makes it possible to handle $0 \leq k^2 \leq 100$ when so desired. To investigate *lmfp* particle and heat transport, however, it is usually deemed sufficient to consider the region $0 \leq k^2 \leq k_u^2$ with a single mesh (where $k_u^2 > 1 + \epsilon_t/\epsilon_h$). The drift equations are those given here in Section II with the following exceptions and/or qualifications.

- It is explicitly assumed that $\epsilon = \epsilon_t = r/R_0$.
- For localized particles it is assumed that $\kappa = \mu B_0$ and terms which are $\mathcal{O}(\epsilon_t, \epsilon_h)$ are ignored.
- As was pointed out in Section II, the expression for $\langle \dot{k}^2 \rangle_r$ lacks the term containing Ω_E. (This oversight occurred due to the premature approximation $R = R_0$; the correct derivation is given here in the Appendix.)

• For non-localized particles, the perpendicular drift terms are considered negligible compared to the rapid motion along **B**; explicitly, $\langle\dot{\theta}\rangle_f = \iota\langle u\rangle/R$, $\langle\dot{\theta}\rangle_b = -\iota\langle u\rangle/R$, and $\langle\dot{k}^2\rangle_{f,b} = -(\epsilon_t/2\epsilon_h)\sin\theta\,\langle\dot{\theta}\rangle_{f,b}$.

One further difference is the presence of a "fictitious drift" — given by $-\Omega_h(\epsilon_t/2\epsilon_h)\cos\theta$ — in the FLOCS expression for $\langle\dot{\theta}\rangle_r$. This term is introduced for numerical purposes to assure that the divergence of the phase-space flow is zero, allowing the kinetic equation to be written in conservation form and thereby insuring the numerical conservation of particles at each time step. An additional assumption is that $\partial\epsilon_h/\partial r = 2\epsilon_h/r$ (a standard analytic approximation for $\ell = 2$ stellarators) and thus $\Omega_h(\epsilon_t/2\epsilon_h) = \Omega_t$. Written explicitly, FLOCS therefore has $\langle\dot{\theta}\rangle_r = \Omega_E + \Omega_h\langle\cos\eta\rangle_r - \Omega_t\cos\theta$. Given the assumptions employed in its linearization, the kinetic equation is valid throughout the entire *lmfp* regime in either of the two limits, $\Omega_E \gg \Omega_t$ or $\Omega_h \gg \Omega_t$. In both of these cases the additional fictitious drift term leads to an $\mathcal{O}(\epsilon)$ change in $\langle\dot{\theta}\rangle_r$ and therefore represents no limitation on the validity of FLOCS. (This modification to $\langle\dot{\theta}\rangle_r$ is made necessary by the ordering of the kinetic equation which eliminates r as a variable from the problem — see the Appendix for a complete discussion of this topic.)

The phase-space flux of particles must also be conserved at the $k^2 = 1$ boundary, requiring that $J_r\langle\dot{k}^2\rangle_r f_r = J_f\langle\dot{k}^2\rangle_f f_f + J_b\langle\dot{k}^2\rangle_b f_b$. This is handled in FLOCS by defining a *trapping probability* so as to be consistent with the flow velocities on either side of the boundary

$$p_t = \lim_{k^2\to 1}\frac{J_r\langle\dot{k}^2\rangle_r}{J_f\langle\dot{k}^2\rangle_f}.$$

To maintain consistency, one must then artificially require $J_b\langle\dot{k}^2\rangle_b = -J_f\langle\dot{k}^2\rangle_f(1-p_t)$. As the trapping probability is very small, this "adjustment" is inconsequential to the physics of the problem; its purpose is numerical, to satisfy the divergence condition and allow finite differencing of the kinetic equation "across" the $k^2 = 1$ boundary. (Note that the GSRAKE equivalent of this condition, $J_r\langle\dot{k}^2\rangle_r f_r + J_f\langle\dot{\zeta}^2\rangle_f f_f + J_b\langle\dot{\zeta}^2\rangle_b f_b = 0$, is automatically satisfied at $k^2 = 1$ since the complete expressions for the drift equations have been retained.)

FLOCS input consists of the simulation parameters, the specification of an appropriate mesh configuration and the assumed values of the solution at each mesh point. The distribution function is then allowed to evolve iteratively over a number of discrete time steps until a steady-state solution is reached; the mesh values of the previous step are used to obtain finite-difference approximations for the derivatives with respect to θ and k^2. In the inaugural run, the distribution function is initialized as a Maxwellian at

every mesh point; subsequent runs employing the same mesh may be initialized with a previous solution (this usually accelerates convergence, especially if the simulation parameters are not too dissimilar). In either case, strict particle conservation is enforced at each time step, stipulating that the non-Maxwellian portion of the solution be neither a source nor a sink of particles. The GSRAKE equivalent of this requirement is given in equation (7).

Numerical stability constraints set a limit on the maximum time step which can be tolerated in an explicit scheme. At the more collisional end of the *lmfp* regime this limit is dictated by the numerical propagation speed of the diffusive flow, but for small values of ν the drift motion becomes the determining factor. In the former case, computational time is independent of the collision frequency; in the latter it is proportional to ν^{-1}. An additional consideration is the increasing localization of the distribution function observed with decreasing ν, demanding ever-finer meshes to obtain the necessary resolution. As a consequence, FLOCS can become prohibitively time consuming for studies of neoclassical transport deep into the *lmfp* regime.

V. COMPARISON OF RESULTS

The analytic theory of *lmfp* neoclassical transport in stellarators exists as a patchwork of results, each one valid for a particular set of assumptions. Broadly speaking, these assumptions concern the relative magnitudes of ν_{eff} and $\Omega_\theta = \Omega_E + \Omega_{\nabla B}$, where ν_{eff} is the effective collision frequency and Ω_θ the poloidal precessional frequency of localized particles due to the $\mathbf{E}\times\mathbf{B}$ and ∇B drifts. Three limiting cases have been investigated: (1) $\nu_{eff} > \Omega_\theta$, the more collisional end of the *lmfp* regime where the relative magnitudes of Ω_E and $\Omega_{\nabla B}$ are unimportant; (2) $\nu_{eff} < \Omega_\theta$, $\Omega_E \gg \Omega_{\nabla B}$; and (3) $\nu_{eff} < \Omega_\theta$, $\Omega_E = 0$ with the additional stipulation $\epsilon_h \gg \epsilon$ (the case $\epsilon_h \lesssim \epsilon$ leads to loss-cone behavior [24] and is not considered here). Numerical studies have been heretofore confined to (1) and (2) since these two cases are generally considered to be most relevant to present and future stellarator experiments.

GSRAKE solutions for the perturbed distribution function are presented in this section which have been chosen so as to consider each of these limiting cases in turn. Plots of the monoenergetic diffusion coefficient as a function of collision frequency are also provided, illustrating the use of GSRAKE for determining neoclassical transport coefficients. Where possible, comparisons are undertaken with the results of other numerical approaches and with the expectations of analytic theory.

A classical $\ell = 2$, $p = 12$ stellarator field with reactor dimensions is used for illustration purposes. Other parameters for the base case are: major radius $R_0 = 20$ m, plasma minor radius $a = 2$ m, magnetic field on axis $B_0 = 4$ T. The flux surface $r = 1$ m is considered, with rotational transform $\iota = 1.47$ and with $\epsilon = 0.05$, $\epsilon_h = 0.063$. Conforming to the assumptions used in the FLOCS code, $\epsilon = \epsilon_t$, $\epsilon_h \propto r^2$, and thus $\partial\epsilon_h/\partial r = 0.126$ (but $\partial\epsilon/\partial r = -0.05$ so as to mimic the fictitious drift present in FLOCS). Results for particles with a kinetic energy corresponding to $T = 12$ keV are presented. For the large electric field cases it is assumed that $\Omega_E = 1875$ s^{-1}; in comparison $\Omega_h = \pm 378$ s^{-1} and $\Omega_t = \mp 150$ s^{-1} (where the upper sign is for protons and the lower sign for electrons). For the $\Omega_E = 0$ results the major radius is increased to $R_0 = 40$ m, leading to the changes $\epsilon = 0.025$ and $\Omega_t = \mp 75$ s^{-1}.

— *(a) The Distribution Function*

Before considering the specific details of individual solutions, some general comments are in order which pertain to all the examples presented here. For GSRAKE simulations, a value of m_{max} must be chosen at which the Fourier representation of f, given in equation (6), is then truncated. This choice presents the usual dilemma; the accuracy of the solution improves with increasing m_{max} but computational speed suffers greatly. These aspects are investigated here by comparing the solutions at different values of m_{max} for $C^{(0)}$, $S^{(1)}$ and $C^{(1)}$, the Fourier coefficients of the primary poloidal harmonics. (Poloidal harmonics which appear in the ripple-averaged drift equations are considered "primary" since any solution of the kinetic equation must contain at least these harmonics.) The results for $S^{(1)}$ are of particular interest since they alone are responsible for the neoclassical particle and heat fluxes (due to the $\sin\theta$ dependence of the radial drift velocity). Results from the FLOCS code are provided for comparison in each case as well. These have been Fourier decomposed so as to conform with the GSRAKE ansatz for the distribution function given in equation (6). The CPU time consumed in the course of a simulation, τ_{CPU}, is an important measure of a numerical solution's efficacy and is provided here for each example. All results were obtained using a CRAY Y-MP computer of the Cray Research Corporation. As a final comment, it should also be mentioned that the FLOCS output plotted for $C^{(0)}$ has been "shifted" by an amount $\Delta C^{(0)}$ to compensate for the neglect of the portion of velocity space $k^2 > k_u^2$. (This shift is without physical consequences and has been done here only to simplify visual comparison of the numerical results.)

Figure 1 presents the solution of the ripple-averaged kinetic equation for protons with $\nu_{eff} = 5625\ \mathrm{s}^{-1}$, illustrating the case $\nu_{eff} > \Omega_\theta$. The left half of each plot depicts the results for localized particles ($0 \leq k^2 < 1$), the right half for non-localized particles ($1 > \zeta^2 \geq 0$). GSRAKE curves are given for $m_{max} = 3$ (solid line), $m_{max} = 2$ (dotted line) and $m_{max} = 1$ (dashed line). These three curves are essentially identical, indicating that accurate results are obtained even when the Fourier series for the perturbed distribution function are truncated at the $m = 1$ terms. FLOCS output is shown by the solid circles ($\bullet$) for f_r and f_f and by the open circles ($\circ$) for f_b. These particular FLOCS results were obtained on a single mesh with $n_\theta = 20$ and $n_k = 60$ (with mesh spacings $\Delta\theta = 2\pi/n_\theta$ and $\Delta k^2 = k_u^2/n_k$) for $k_u^2 = 3$ (hence FLOCS output for non-localized particles is confined to the range of pitch-angle values $1 \geq \zeta^2 \geq 1/3$).

An analytic solution of the ripple-averaged kinetic equation for localized particles may be derived in this case as well, employing an ordering scheme in the small quantity Ω_θ/ν_{eff}. The lowest-order solution is

$$f_r = \frac{v_d}{\nu_{eff}} \frac{\epsilon}{\epsilon_t} (k^2 - 1) \sin\theta \frac{\partial F_m}{\partial r} + \mathcal{K}(\theta),$$

where $\mathcal{K}$ is a constant with respect to k^2, to be determined by the boundary conditions at $k^2 = 1$. In the literature it is often argued that one may assume $f_f = f_b = 0$ in the *lmfp* regime, the so-called *Maxwellian* approximation, and hence $\mathcal{K} = 0$. Alternately, one supposes the radial drift displacement of non-localized particles to be negligibly small in the *lmfp* regime — the *zero-banana-width* approximation — and finds solutions for f_f and f_b which are even functions of θ [25]. On the basis of either assumption, one obtains the boundary condition $S_r^{(1)}(k^2 = 1) = 0$.

Checking these analytic approximations against the numerical results of figure 1, however, it must immediately be concluded that the agreement is poor. Although $S_r^{(1)}$ is indeed a linear function of k^2, its value at the $k^2 = 1$ boundary is far removed from zero. Further, the solutions for the forward and backward distribution functions are by no means even functions of θ, much less Maxwellian. In fairness, it should be pointed out that the current example has $\tau_b \nu_{eff} \approx 1/3$, and is thus in the *lmfp* regime but at its collisional end. To investigate whether the analytic approximations are more appropriate deeper into the *lmfp* regime, the identical set of parameters is reconsidered for electrons ($\tau_b \nu_{eff} < 0.01$); results may be found in figure 2. In this example the analytic expectations for $S_r^{(1)}$ are verified by the numerical results. The solutions for non-localized particles are again non-Maxwellian but are, to good approximation, even functions of θ.

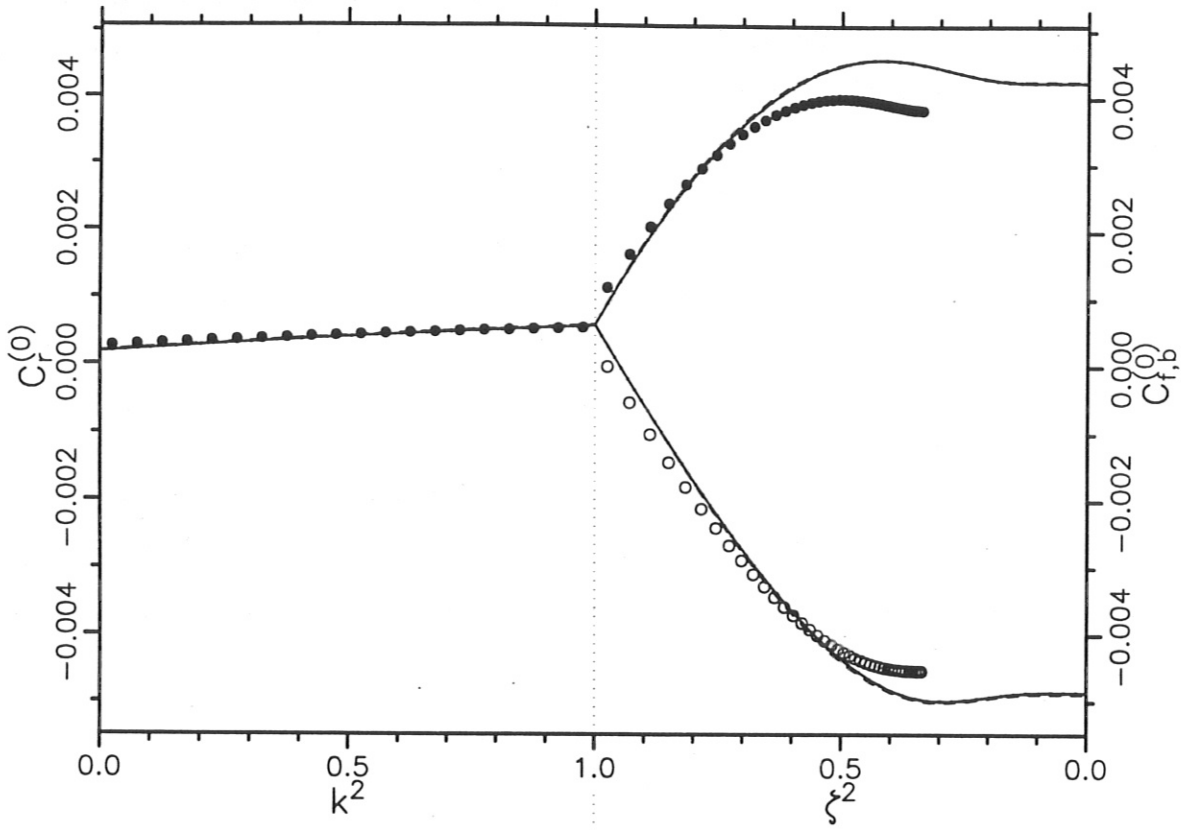
0.004
0.002
0.000
−0.002
−0.004
$C_r^{(0)}$
$C_{f,b}^{(0)}$
0.0
0.5
1.0
k^2
ζ^2

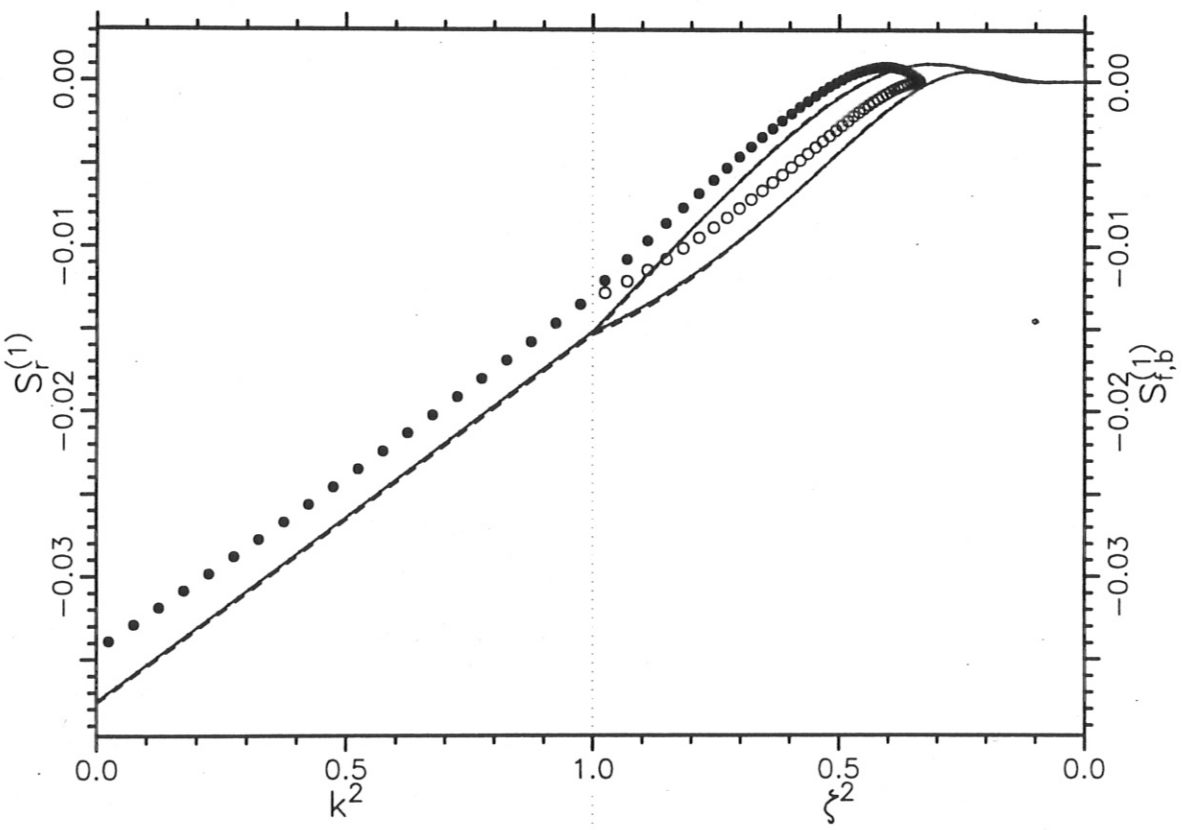
0.00
−0.01
−0.02
−0.03
$S_r^{(1)}$
$S_{f,b}^{(1)}$
0.0
0.5
1.0
k^2
ζ^2

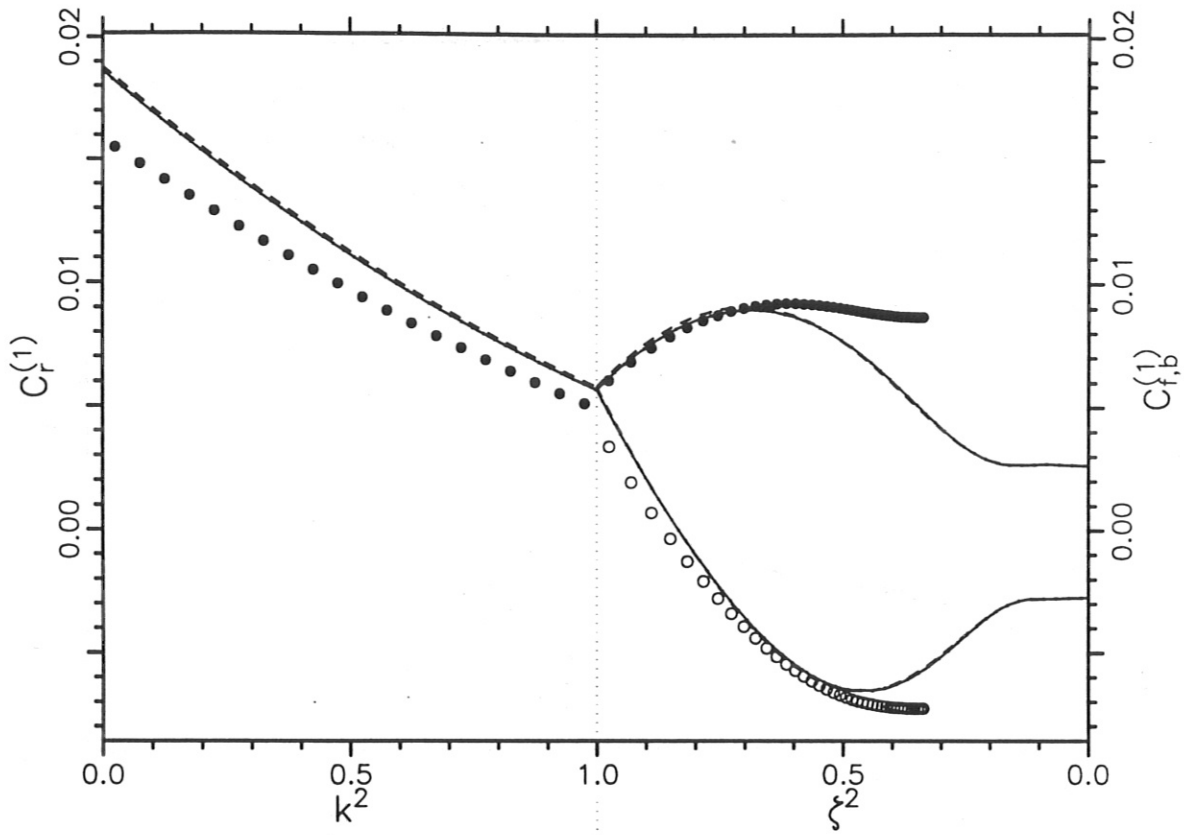

Figure 1. Numerical solutions of the ripple-averaged kinetic equation are presented for the $m = 0$ and $m = 1$ Fourier coefficients of the perturbed distribution function of *protons*. The left half of each plot depicts the results for ripple-localized particles (components of f_r), the right half for non-localized particles (components of f_f and f_b). The simulation parameters are $v_d = 150$ m/s, $\nu_{eff} = 5625$ s^{-1}, $\Omega_E = 1875$ s^{-1}, $\Omega_h = 378$ s^{-1} and $\Omega_t = -150$ s^{-1}. GSRAKE solutions are shown for $m_{max} = 3$ (solid line, $\tau_{CPU} = 0.95$ s), $m_{max} = 2$ (dotted line, $\tau_{CPU} = 0.40$ s) and $m_{max} = 1$ (dashed line, $\tau_{CPU} = 0.12$ s). The number of nodes in each case is $n = 27$. FLOCS results were determined using a single mesh with $n_\theta = 20$, $n_k = 60$ and $k_u^2 = 3$ and are plotted as solid circles (•) for f_r and f_f and as open circles (○) for f_b. An offset of $\Delta C^{(0)} = 3.0 \times 10^{-4}$ has been added to the FLOCS solution for $C^{(0)}$ to compensate for the neglect of the portion of velocity space $k^2 > k_u^2$. The computational time required was $\tau_{CPU} = 105$ s.

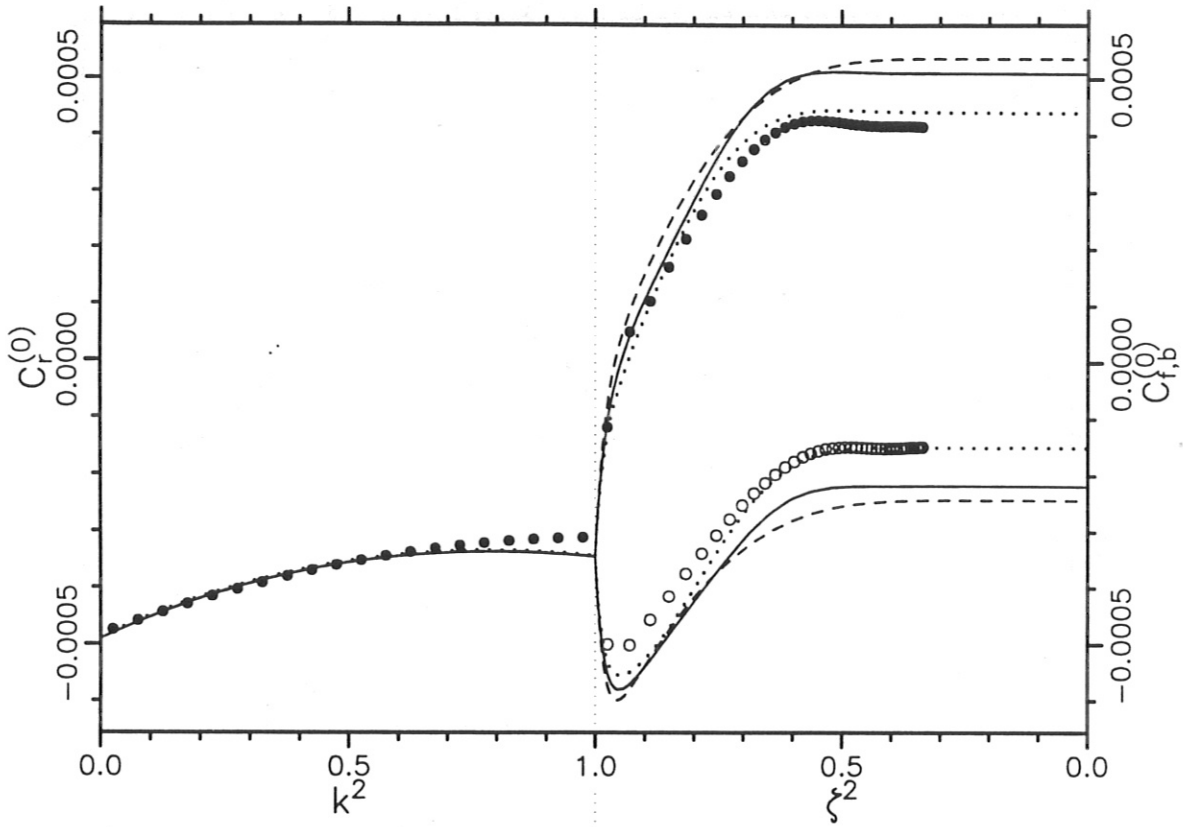
0.0005
0.0000
−0.0005
$C_r^{(0)}$
$C_{f,b}^{(0)}$
0.0
0.5
1.0
k^2
ζ^2

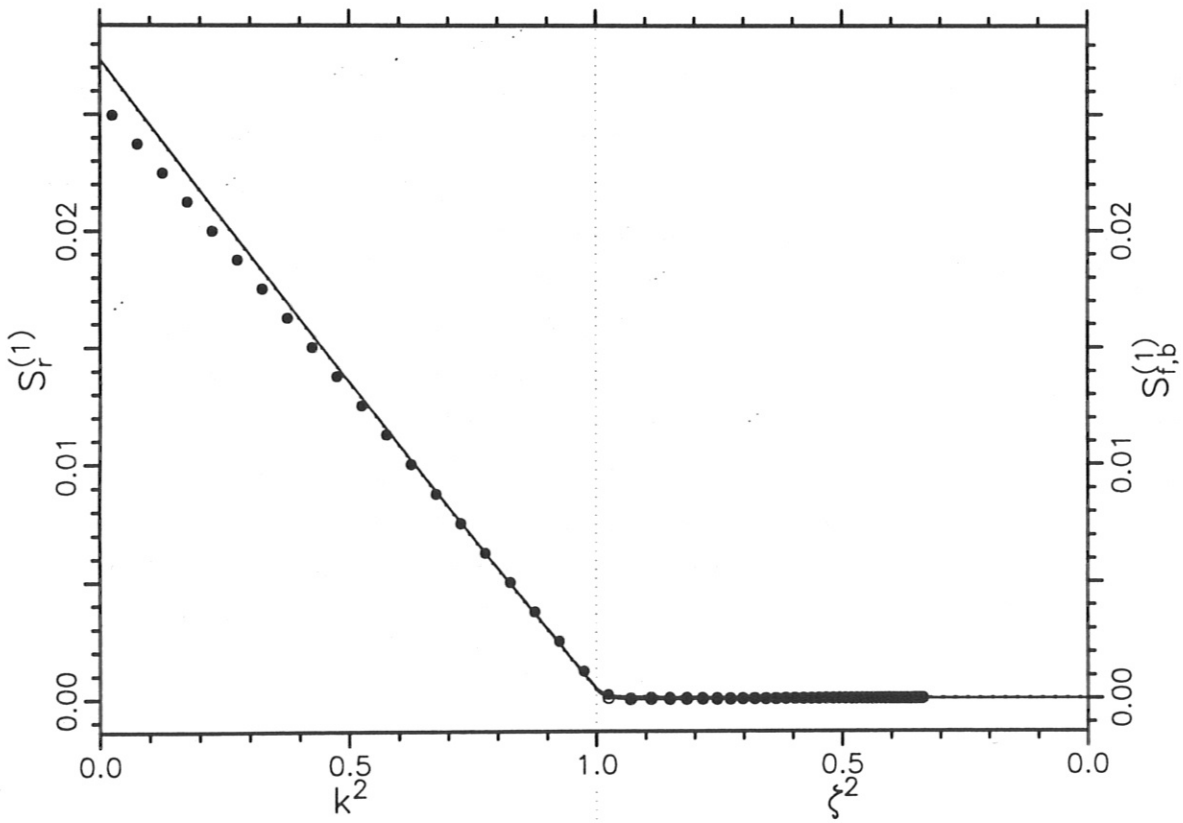
0.02
0.01
0.00
$S_r^{(1)}$
$S_{f,b}^{(1)}$
0.0
0.5
1.0
k^2
ζ^2

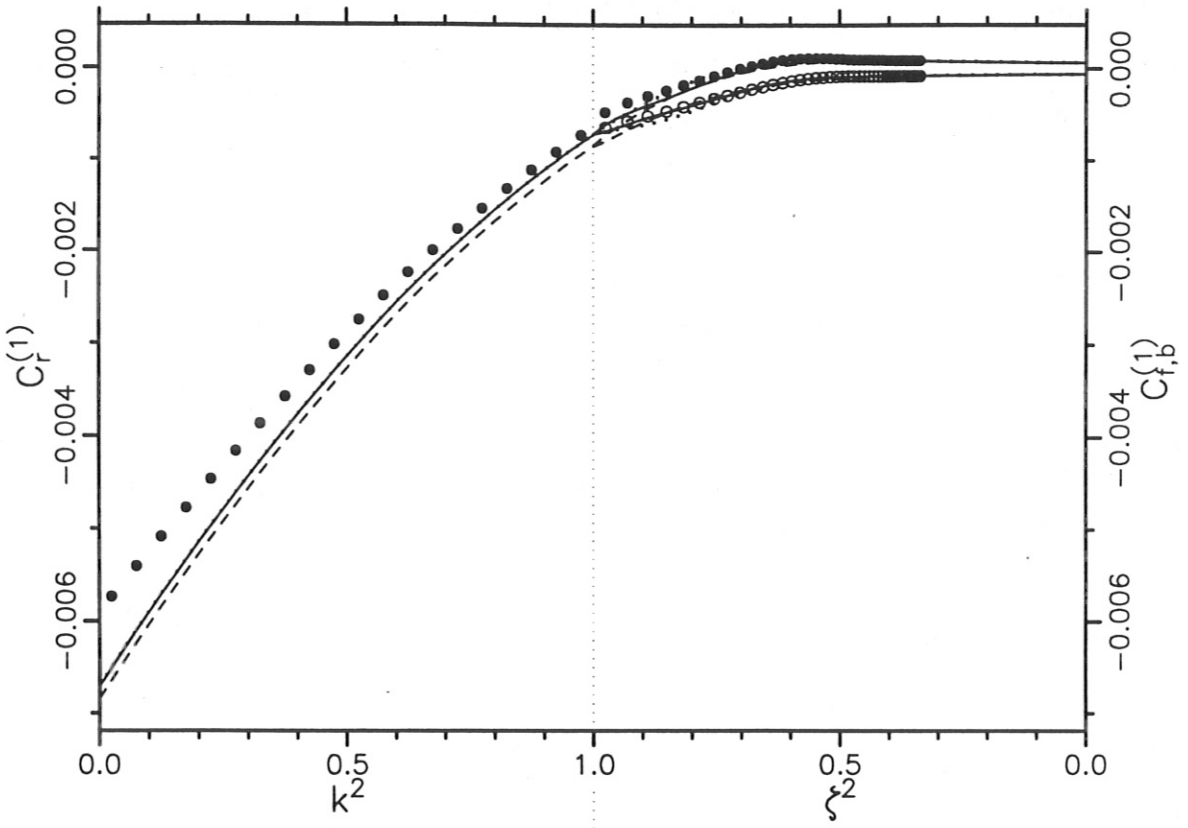

Figure 2. Numerical solutions of the ripple-averaged kinetic equation are presented for the $m = 0$ and $m = 1$ Fourier coefficients of the perturbed distribution function of *electrons*. The left half of each plot depicts the results for ripple-localized particles (components of f_r), the right half for non-localized particles (components of f_f and f_b). The simulation parameters are $v_d = -150$ m/s, $\nu_{eff} = 5625$ s^{-1}, $\Omega_E = 1875$ s^{-1}, $\Omega_h = -378$ s^{-1} and $\Omega_t = 150$ s^{-1}. GSRAKE solutions are shown for $m_{max} = 3$ (solid line, $\tau_{CPU} = 1.95$ s), $m_{max} = 2$ (dotted line, $\tau_{CPU} = 0.85$ s) and $m_{max} = 1$ (dashed line, $\tau_{CPU} = 0.25$ s). The number of nodes in each case is $n = 36$. FLOCS results were determined using a single mesh with $n_\theta = 20$, $n_k = 60$ and $k_u^2 = 3$ and are plotted as solid circles (•) for f_r and f_f and as open circles (○) for f_b. An offset of $\Delta C^{(0)} = -1.5 \times 10^{-4}$ has been added to the FLOCS solution for $C^{(0)}$ to compensate for the neglect of the portion of velocity space $k^2 > k_u^2$. The computational time required was $\tau_{CPU} = 70$ s.

Approximate or assumed solutions for f_f and f_b are a standard feature of most analytic theories of *lmfp* transport in stellarators. The results presented in figures 1 and 2 have demonstrated that such solutions are appropriate under certain circumstances but not in the general case. Complete and accurate solutions of the kinetic equations for non-localized particles are therefore indispensable to a comprehensive description of neoclassical transport. Further emphasis of this point is found on examination of the numerical solutions given in figure 1. Here, the FLOCS results were determined using a single mesh with $k_u^2 = 3$, and show clear differences in comparison to the GSRAKE curves. The agreement is significantly improved, however, if the amount of pitch-angle space covered by the FLOCS solution is expanded, e.g., using seven meshes with $k_u^2 = 90$. Unfortunately, the price paid for this improvement is high; FLOCS computational time is increased by a factor of four in this example.

In figure 3, the collision frequency has been reduced by an order of magnitude to consider the case $\nu_{eff} < \Omega_\theta$, $\Omega_E \gg \Omega_{\nabla B}$ for protons. The favorable effect Ω_E has on the confinement of deeply trapped particles is clearly exhibited in this example by a strong reduction in the magnitude of $S_r^{(1)}$ for small values of k^2. The GSRAKE results remain relatively insensitive to the value of m_{max}, although the plots do show that small inaccuracies are introduced into the solution if the Fourier series are truncated at the $m = 1$ terms. An important rule of thumb for FLOCS simulations is also illustrated in figure 3; distortions of the results are avoided only if the solution is a constant (or nearly constant) function of pitch angle in the portion of velocity space excluded from the simulation. For the current example, a single mesh with $k_u^2 = 3$ is sufficient to obtain good agreement with GSRAKE results. The reader's attention is again drawn to the complex nature of the solutions for f_f and f_b near the $k^2 = 1$ boundary, which defy any simple analytic approximation.

Further characteristics of the numerical solutions are revealed by moving yet deeper into the *lmfp* regime; an example is provided by figure 4, in which $\nu_{eff} = 56.25\ \mathrm{s}^{-1}$. Two trends are discernible. First, the solution for $S^{(1)}$ becomes increasingly localized near the $k^2 = 1$ boundary, and, second, the GSRAKE results become more sensitive to the value of m_{max} used in the simulation. Nevertheless, even when considering the smallest physically relevant values of ν_{eff}, $m_{max} = 3$ is sufficient to obtain accurate results with GSRAKE, and computational times never exceed five seconds. The increasing localization of the distribution function with decreasing collision frequency has more serious consequences for FLOCS simulations, however. In the current example, erratic fluctuation of the solutions for $S_f^{(1)}$ and $S_b^{(1)}$ is observed near $k^2 = 1$, even though the

k^2 resolution has been increased by choosing a mesh with $n_k = 90$ (the fluctuation is much more pronounced for $n_k = 60$ and affects the accuracy of the results accordingly). Further localization of the solution at smaller ν demands yet finer meshes and ultimately leads to excessive values of τ_{CPU}.

The final comparison of solutions undertaken here is depicted in figure 5 as an example of the case $\nu_{eff} < \Omega_\theta$, $\Omega_E = 0$. The major radius used in these simulations has been increased to $R_0 = 40$ m as a means of better satisfying the requirement $\Omega_h \gg \Omega_t$. Even so, the magnitude of the solution for localized particles is perhaps greater than one would wish, given the assumption $f_r \ll F_m$ which underlies the derivation of the ripple-averaged kinetic equation.

— (b) The Monoenergetic Diffusion Coefficient

Once the solution for the perturbed distribution function has been determined, it is straightforward to calculate the associated neoclassical particle and heat fluxes

$$\begin{bmatrix} \Gamma \\ Q \end{bmatrix} = -4\pi \left(\frac{2}{m^3}\right)^{1/2} \int_0^\infty d\kappa \begin{bmatrix} \kappa^{1/2} \\ \kappa^{3/2} \end{bmatrix} D(\kappa) \frac{\partial F_m}{\partial r},$$

where the monoenergetic diffusion coefficient is given by

$$D(\kappa) = -\frac{v_d}{\pi}\frac{\epsilon}{\epsilon_t}\left(\frac{\epsilon_h}{2}\right)^{1/2} \int_0^1 dk^2\, S_r^{(1)} \left(\frac{\mu B_0}{\kappa}\right)^{3/2} \left(K(k) + \epsilon_h \frac{\mu B_0}{\kappa}\frac{A(k^2)}{4}\right)$$

$$-\frac{v_d}{2\pi}\frac{\epsilon}{\epsilon_t}\left(\frac{\epsilon_h}{2}\right)^{1/2} \int_0^1 d\zeta^2\, (S_f^{(1)} + S_b^{(1)}) \left(\frac{\mu B_0}{\zeta^2\kappa}\right)^{3/2} \left(K(\zeta) + 2\epsilon_h \frac{\mu B_0}{\zeta^2\kappa} E(\zeta)\right).$$

The terminology "monoenergetic" is employed here to distinguish $D(\kappa)$ from the "true" diffusion coefficient, which, by convention, multiplies the density gradient in the energy-integrated expression for the particle flux. The utility of $D(\kappa)$ lies in the fact that it is a quantity which may be easily determined from a number of different numerical simulations and thereby provides a convenient basis for comparison. In what follows, such comparisons are provided for results from GSRAKE, FLOCS, a Monte Carlo simulation of neoclassical transport and the DKES code. Prior to this undertaking, however, a short digression is necessary to provide a brief description of the latter two numerical approaches.

Orbit-following Monte Carlo codes have been traditionally among the most widely used numerical tools for investigating neoclassical transport in stellarators. Such codes exist in considerable number, of which the references given here [13-18] represent only a small sample. The Monte Carlo results presented in this paper were determined by a

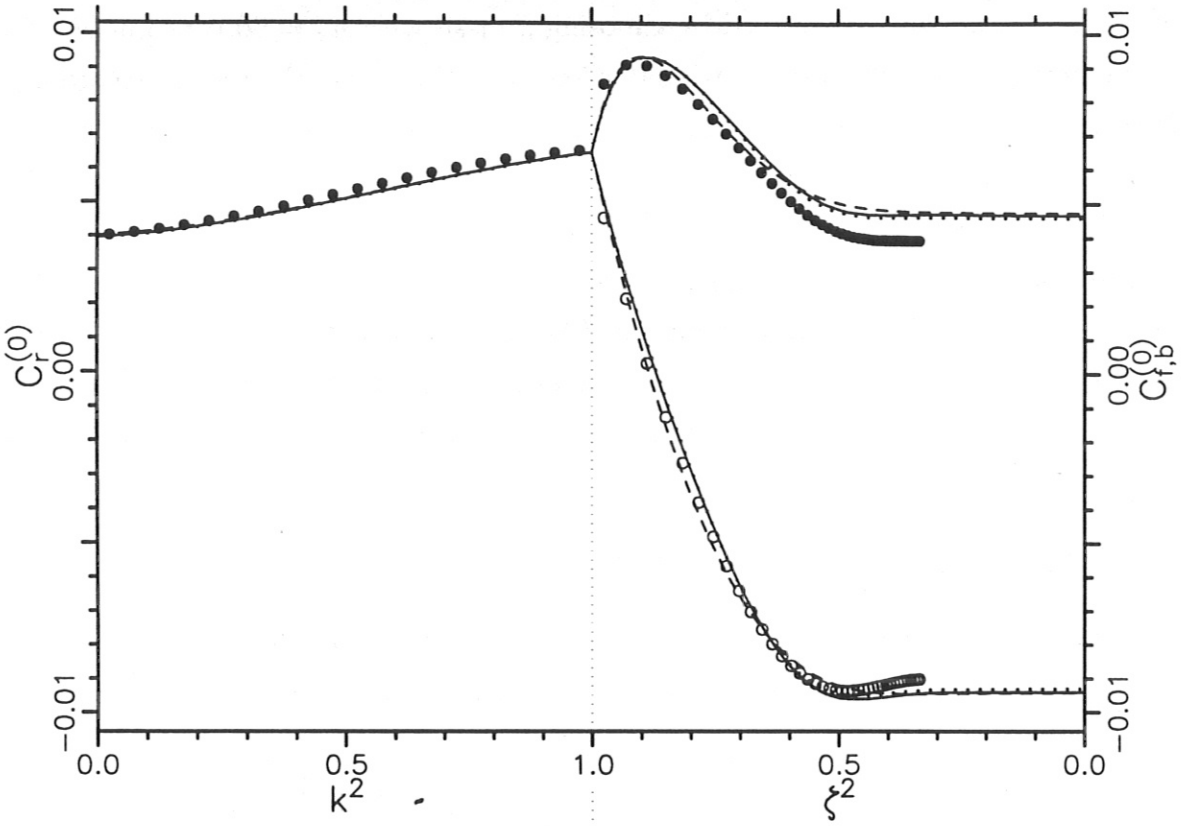
0.01
0.00
−0.01
$C_r^{(0)}$
$C_{f,b}^{(0)}$
0.0
0.5
1.0
k^2
ζ^2

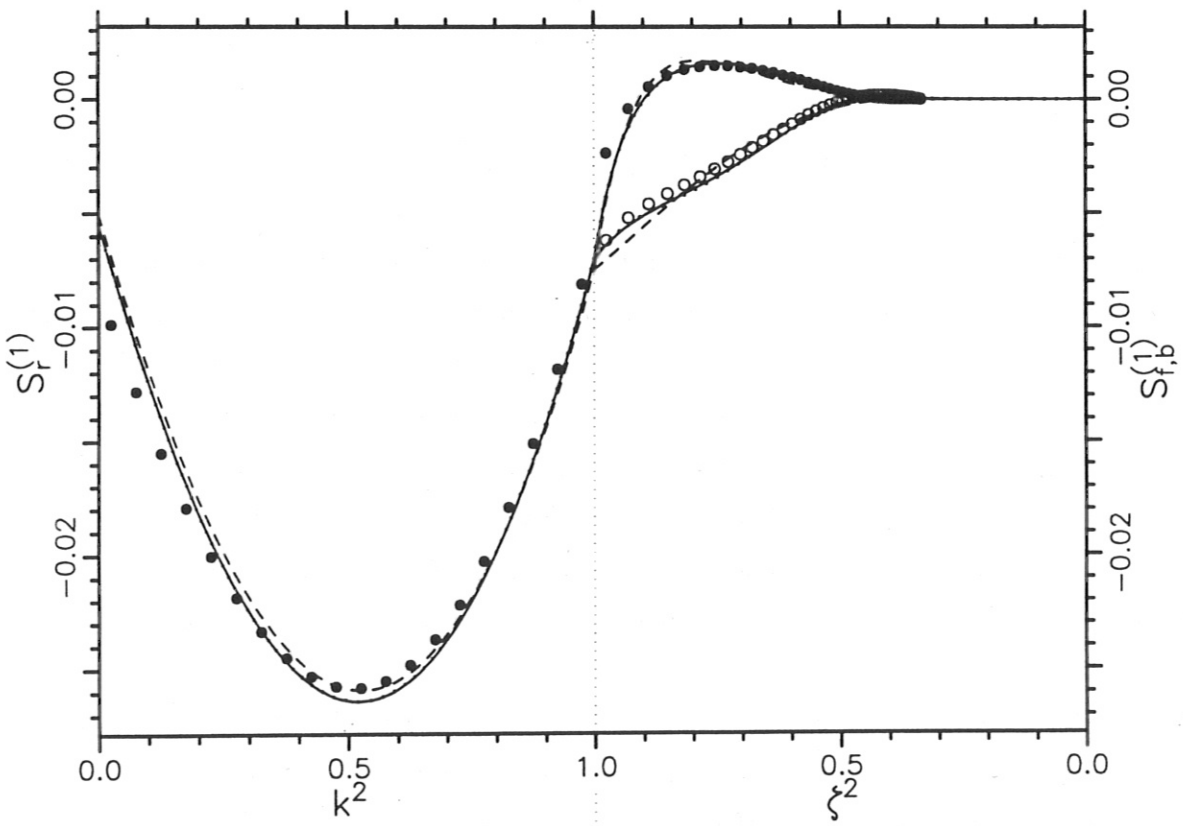
0.00
−0.01
−0.02
$S_r^{(1)}$
$S_{f,b}^{(1)}$
0.0
0.5
1.0
k^2
ζ^2

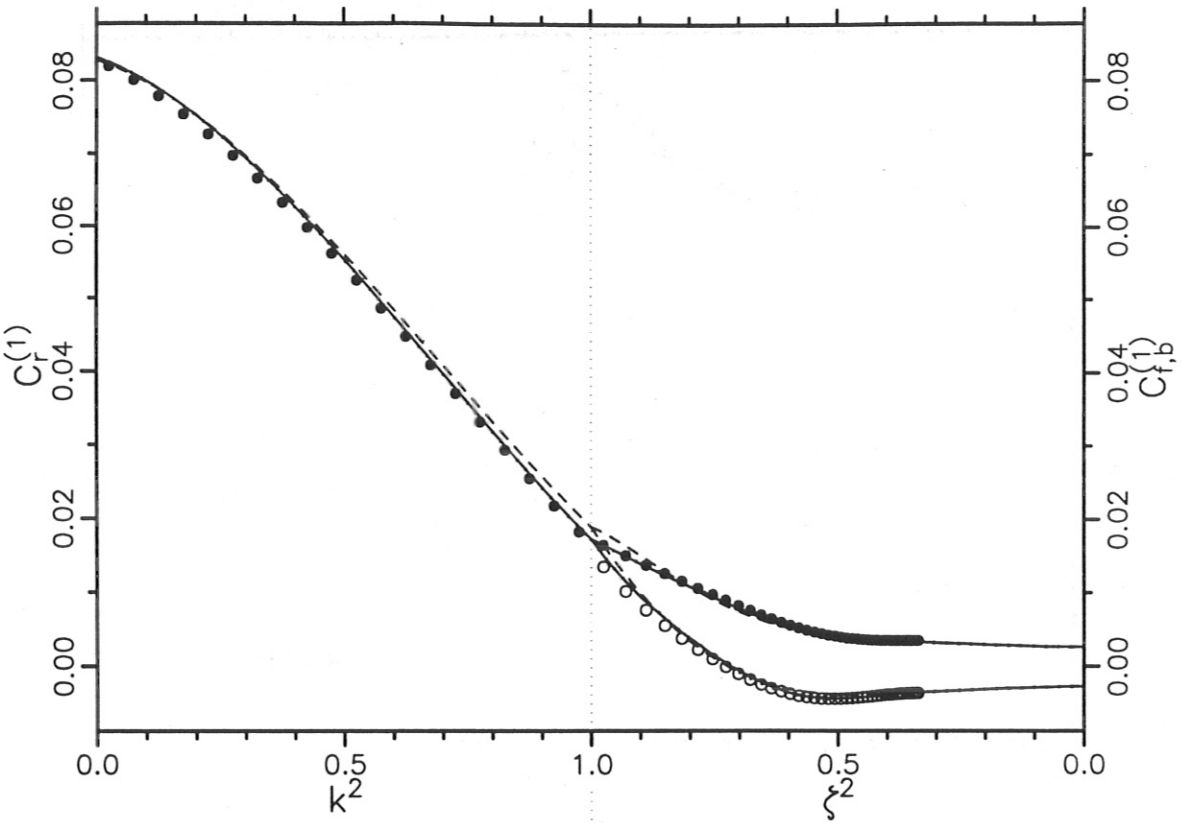

Figure 3. Numerical solutions of the ripple-averaged kinetic equation are presented for the $m = 0$ and $m = 1$ Fourier coefficients of the perturbed distribution function of *protons*. The left half of each plot depicts the results for ripple-localized particles (components of f_r), the right half for non-localized particles (components of f_f and f_b). The simulation parameters are $v_d = 150$ m/s, $\nu_{eff} = 562.5$ s^{-1}, $\Omega_E = 1875$ s^{-1}, $\Omega_h = 378$ s^{-1} and $\Omega_t = -150$ s^{-1}. GSRAKE solutions are shown for $m_{max} = 3$ (solid line, $\tau_{CPU} = 1.50$ s), $m_{max} = 2$ (dotted line, $\tau_{CPU} = 0.65$ s) and $m_{max} = 1$ (dashed line, $\tau_{CPU} = 0.19$ s). The number of nodes in each case is $n = 32$. FLOCS results were determined using a single mesh with $n_\theta = 20$, $n_k = 60$ and $k_u^2 = 3$ and are plotted as solid circles (•) for f_r and f_f and as open circles (○) for f_b. An offset of $\Delta C^{(0)} = 2.5 \times 10^{-3}$ has been added to the FLOCS solution for $C^{(0)}$ to compensate for the neglect of the portion of velocity space $k^2 > k_u^2$. The computational time required was $\tau_{CPU} = 105$ s.

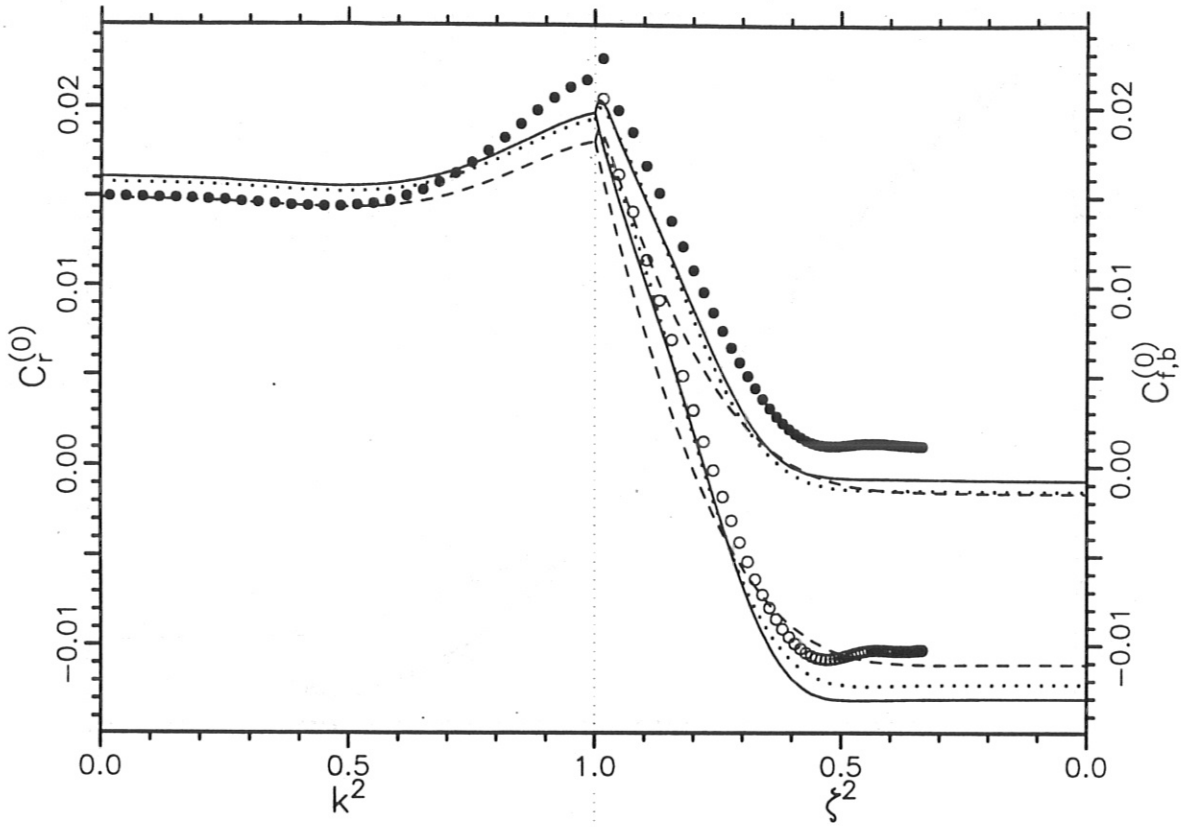
0.02
0.01
0.00
−0.01
$C_r^{(0)}$
$C_{f,b}^{(0)}$
0.0
0.5
1.0
k^2
ζ^2

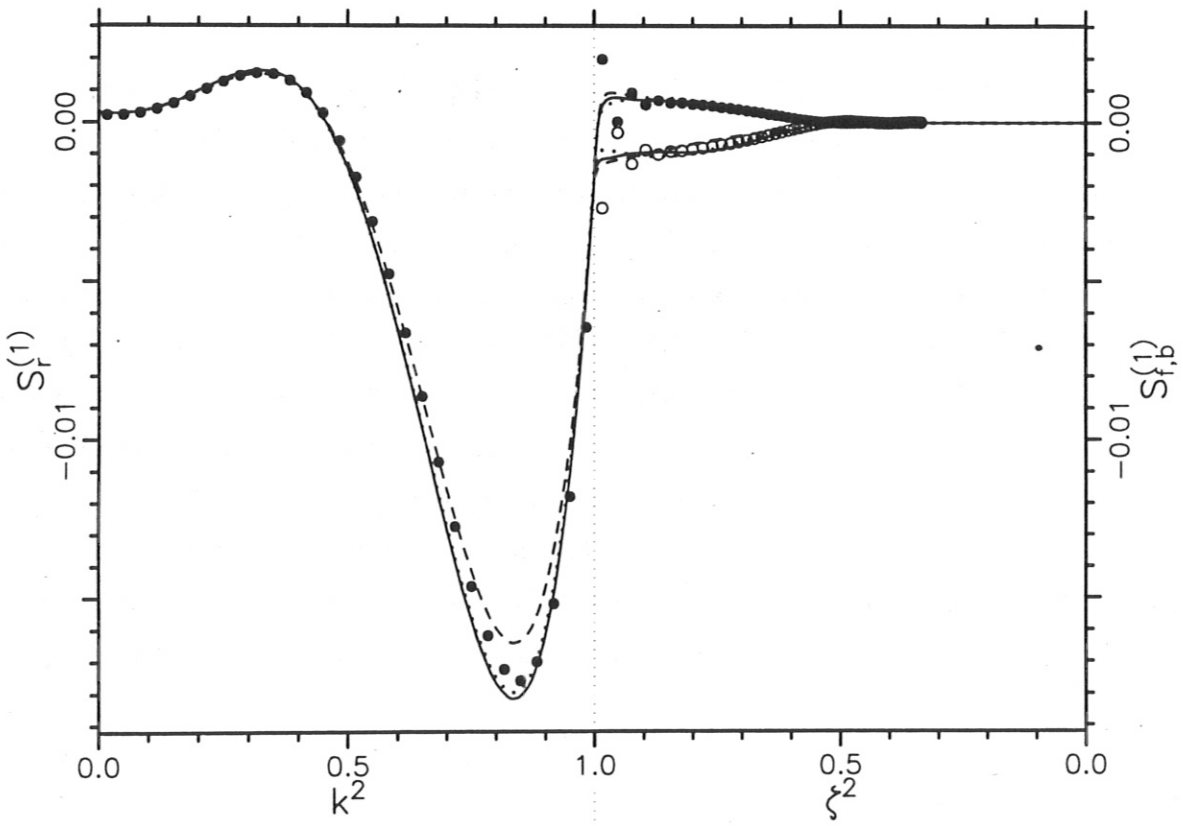
0.00
−0.01
$S_r^{(1)}$
$S_{f,b}^{(1)}$
0.0
0.5
1.0
k^2
ζ^2

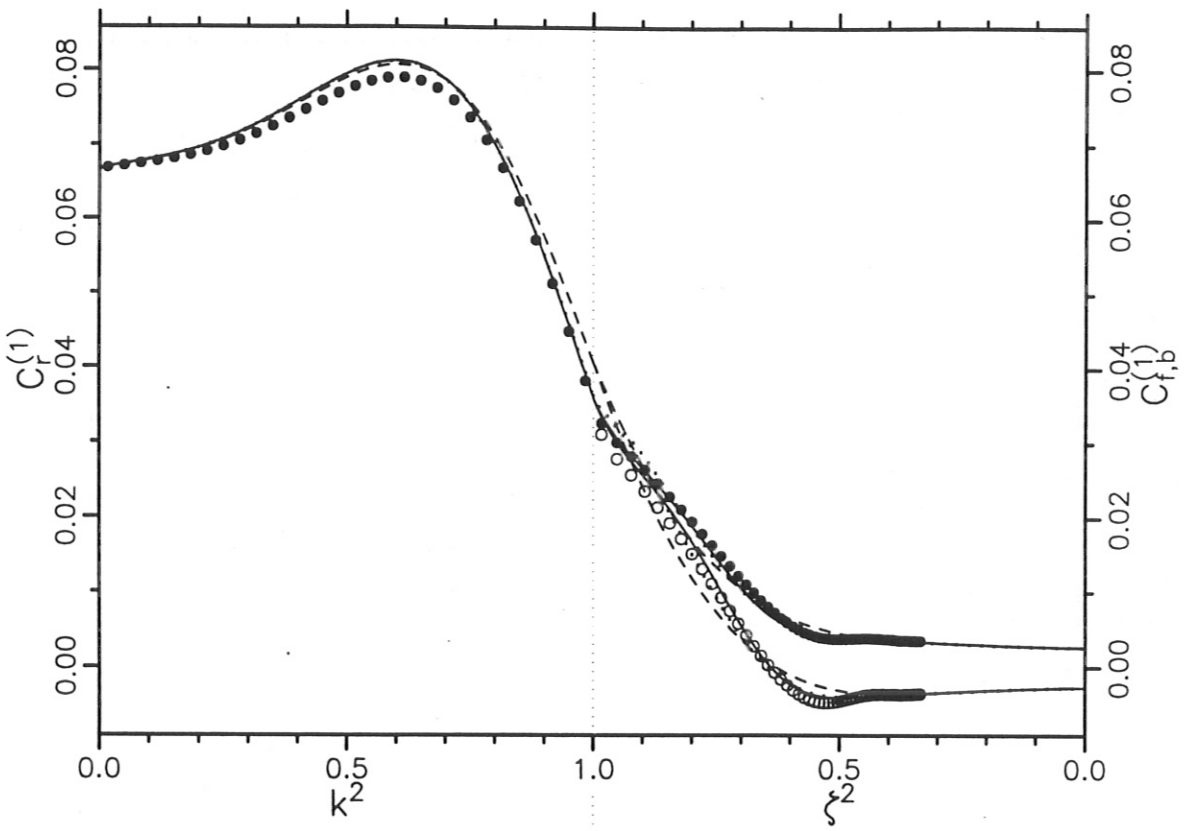

Figure 4. Numerical solutions of the ripple-averaged kinetic equation are presented for the $m = 0$ and $m = 1$ Fourier coefficients of the perturbed distribution function of *protons*. The left half of each plot depicts the results for ripple-localized particles (components of f_r), the right half for non-localized particles (components of f_f and f_b). The simulation parameters are $v_d = 150$ m/s, $\nu_{eff} = 56.25$ s^{-1}, $\Omega_E = 1875$ s^{-1}, $\Omega_h = 378$ s^{-1} and $\Omega_t = -150$ s^{-1}. GSRAKE solutions are shown for $m_{max} = 3$ (solid line, $\tau_{CPU} = 2.20$ s), $m_{max} = 2$ (dotted line, $\tau_{CPU} = 0.95$ s) and $m_{max} = 1$ (dashed line, $\tau_{CPU} = 0.28$ s). The number of nodes in each case is $n = 38$. FLOCS results were determined using a single mesh with $n_\theta = 20$, $n_k = 90$ and $k_u^2 = 3$ and are plotted as solid circles (•) for f_r and f_f and as open circles (○) for f_b. An offset of $\Delta C^{(0)} = 8.5 \times 10^{-3}$ has been added to the FLOCS solution for $C^{(0)}$ to compensate for the neglect of the portion of velocity space $k^2 > k_u^2$. The computational time required was $\tau_{CPU} = 485$ s.

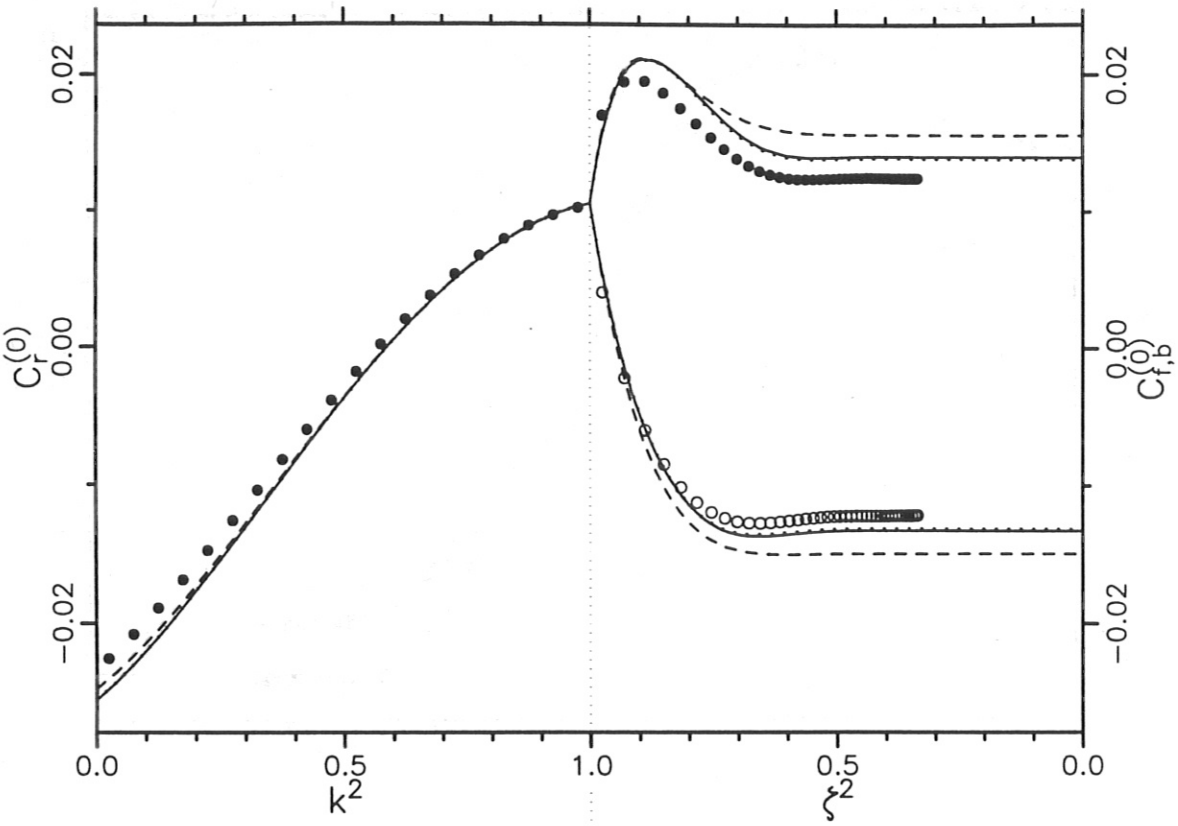
0.02
0.00
−0.02
$C_r^{(0)}$
$C_{f,b}^{(0)}$
0.0
0.5
1.0
k^2
ζ^2

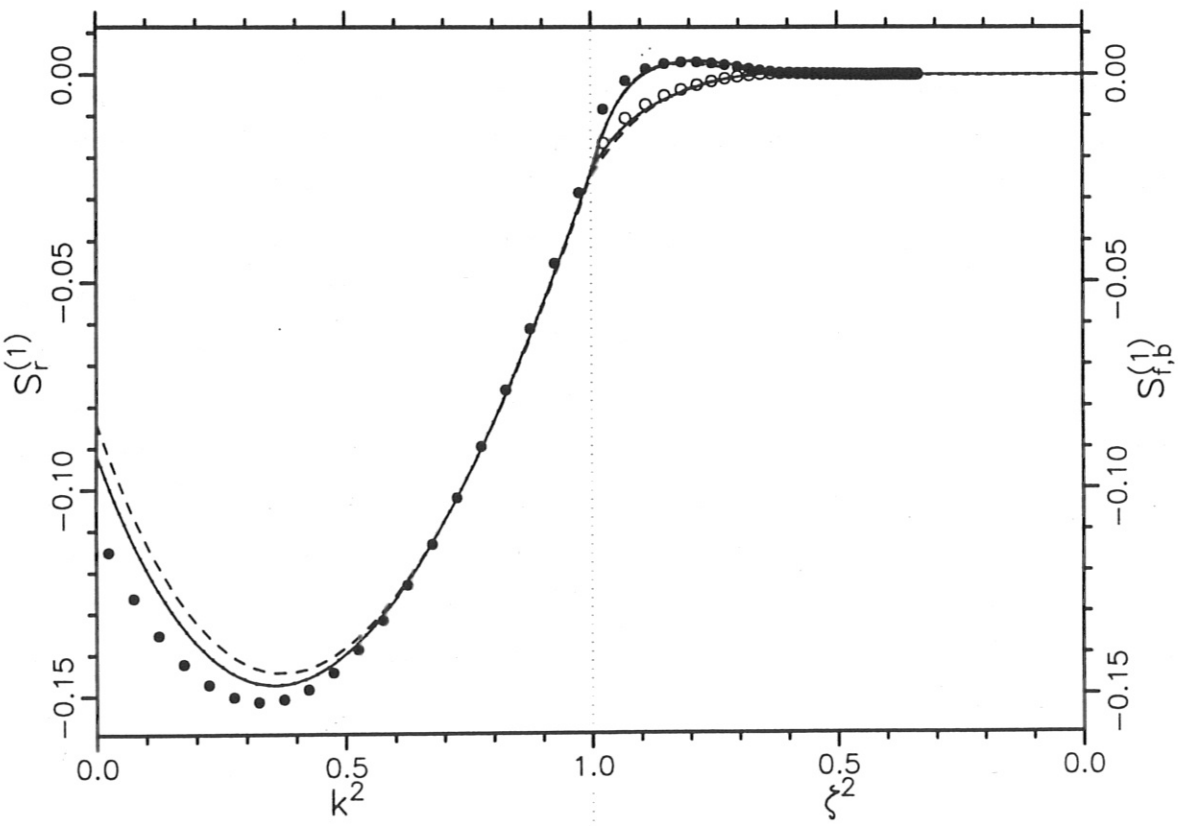
0.00
−0.05
−0.10
−0.15
$S_r^{(1)}$
$S_{f,b}^{(1)}$
0.0
0.5
1.0
k^2
ζ^2

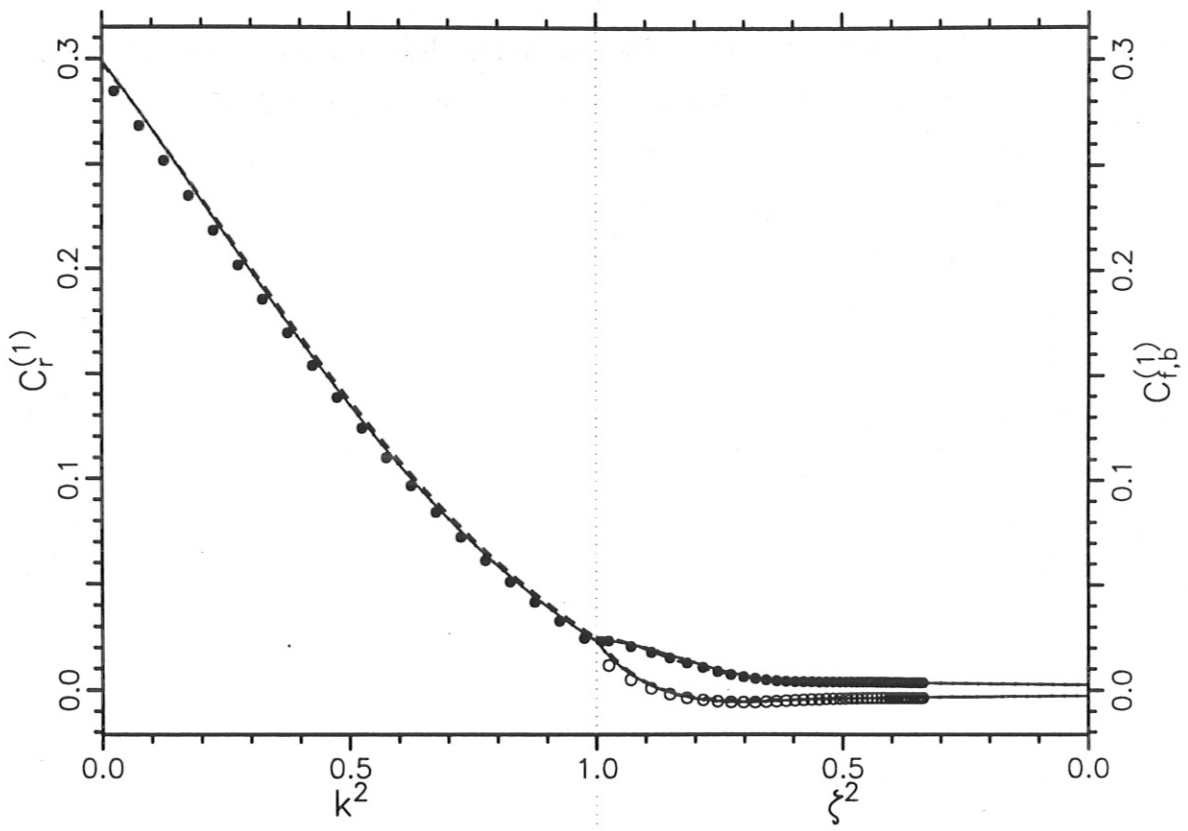

Figure 5. Numerical solutions of the ripple-averaged kinetic equation are presented for the $m = 0$ and $m = 1$ Fourier coefficients of the perturbed distribution function of *protons*. The left half of each plot depicts the results for ripple-localized particles (components of f_r), the right half for non-localized particles (components of f_f and f_b). The simulation parameters are $v_d = 75$ m/s, $\nu_{eff} = 126\ \mathrm{s}^{-1}$, $\Omega_E = 0$, $\Omega_h = 378\ \mathrm{s}^{-1}$ and $\Omega_t = -75\ \mathrm{s}^{-1}$. GSRAKE solutions are shown for $m_{max} = 3$ (solid line, $\tau_{CPU} = 1.70$ s), $m_{max} = 2$ (dotted line, $\tau_{CPU} = 0.70$ s) and $m_{max} = 1$ (dashed line, $\tau_{CPU} = 0.21$ s). The number of nodes in each case is $n = 34$. FLOCS results were determined using a single mesh with $n_\theta = 20$, $n_k = 60$ and $k_u^2 = 3$ and are plotted as solid circles (•) for f_r and f_f and as open circles (○) for f_b. The computational time required was $\tau_{CPU} = 135$ s.

simulation which offers the user three choices for the description of collisionless particle orbits — the numerical integration of a complete set of guiding-center equations of motion (most accurate), the iterative conservation of adiabatic invariants (most efficient computationally), or a "hybrid" combination of these two [18]. All results given here were obtained using the first of these choices. A simulation begins with the launching of monoenergetic test particles on a given flux surface; the initial values of ϕ, θ and pitch angle for each particle are chosen randomly. The particle orbits are then followed numerically over a large number of discrete time steps. After each step the particles undergo pitch-angle scattering according to a numerical algorithm which simulates the effects of the Lorentz collision operator. Statistical estimates of the monoenergetic diffusion coefficient are ultimately determined, based on the final radial positions of all test particles.

DKES is a numerical solution of the linearized drift kinetic equation for arbitrarily complex magnetic-field configurations [21,22] and, as such, avoids all the assumptions and approximations which are necessary to justify ripple averaging. The solution employs a variational principle in which the trial functions are expanded in a Fourier-Legendre series. Upper and lower bounds for the neoclassical transport coefficients are determined which converge monotonically as the number of Fourier-Legendre harmonics is increased. Within the constraints of computer time and memory it is thus possible to determine these quantities to an arbitrary degree of accuracy. In common with the other numerical simulations, collisional processes are modeled using the Lorentz collision operator. For the current purpose of comparison, DKES does have one shortcoming, however. The method of solution requires a self-adjoint form of the kinetic equation, which is achieved by ignoring the ∇B drift in the equation for $d\theta/dt$; DKES is thus incapable of considering the limiting case $\nu_{eff} < \Omega_\theta$, $\Omega_E = 0$.

Figure 6 presents results from the four numerical simulations for the monoenergetic diffusion coefficient of 12 keV protons as a function of the normalized collision frequency ν_{eff}/Ω_E. GSRAKE results are given by the solid, dotted and dashed curves for m_{max} values of 3, 2 and 1, respectively. Each of these curves is composed of 100 individual data points (20 points per decade). FLOCS output is shown by crosses (+), statistical estimates of D from the Monte Carlo simulation are given as solid circles (•) and DKES results are plotted as open circles (○). Also shown for comparison by the dot-dash line is an analytic estimate for the monoenergetic diffusion coefficient, $D = D_t + D_h$, where

$$D_t = \left(D_{PS}^{3/2} + D_{bp}^{3/2} \right)^{2/3}$$

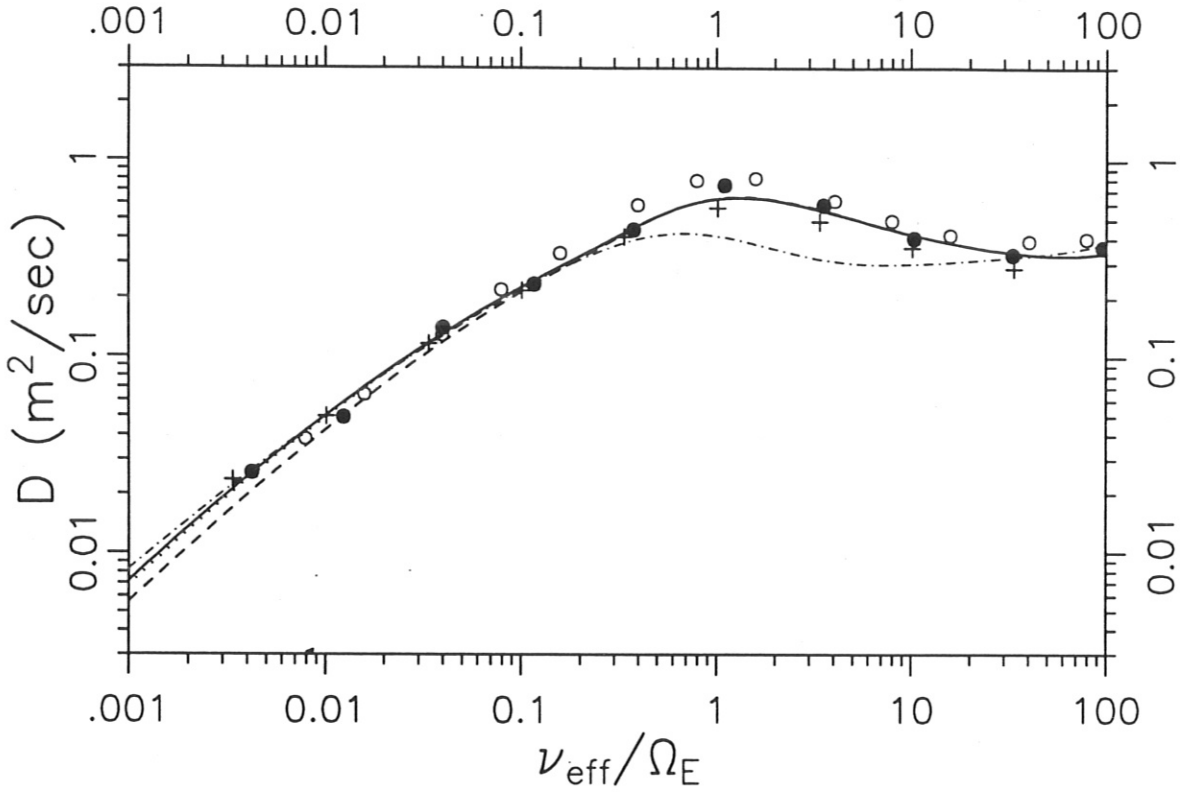

Figure 6. The monoenergetic diffusion coefficient of 12 keV protons is plotted as a function of normalized collision frequency for an $\ell = 2$, $p = 12$ stellarator with $R_0 = 20$ m, $B_0 = 4$ T, $\epsilon = \epsilon_t = 0.05$, $\epsilon_h = 0.063$, $\iota = 1.47$ and $\Omega_E = 1875$ s^{-1}. GSRAKE results are shown for $m_{max} = 3$ (solid line), $m_{max} = 2$ (dotted line) and $m_{max} = 1$ (dashed line). Each of these curves consists of 100 data points (20 points per decade), requiring total CPU times of 180, 79 and 25 seconds, respectively. Results from FLOCS are shown as crosses (+) $\rightarrow$ 9 data points, total $\tau_{CPU} = 4800$ s. Statistical estimates of D from a guiding-center Monte Carlo simulation are given as solid circles (•) $\rightarrow$ 10 data points, total $\tau_{CPU} = 1.8 \times 10^4$ s. DKES results are plotted as open circles (○) $\rightarrow$ 13 data points, total $\tau_{CPU} = 2350$ s. An analytic approximation for D given in the text is shown by the dot-dash line.

in which

$$D_{PS} = \frac{7}{5}\left\{\left(\frac{\epsilon}{\epsilon_t}\right)^2 + \left(\frac{\epsilon_h}{\epsilon_t}\right)^2\left(\frac{\ell_t}{\ell_t - p}\right)^2\right\}\frac{v_d R_0}{\Omega_t{}^2}\,\nu\,,$$

$$D_{bp} = \frac{D_b D_p}{(D_b + D_p)}\,,$$

$$D_p = \frac{2}{5}\left\{\left(\frac{\epsilon}{\epsilon_t}\right)^2 + \left(\frac{\ell\epsilon_h}{\epsilon_t}\right)^2\frac{t}{|\ell_t - p|}\right\}\frac{v_d v}{\Omega_t}\,,$$

$$D_b = \left\{\frac{\epsilon^{1/2}}{\epsilon_t^2} + \frac{\epsilon_h^{1/2}}{\epsilon_t^2}\left(\frac{\ell_t}{\ell_t - p}\right)^2\right\}\frac{v_d R_0}{\Omega_t{}^2}\,\nu\,,$$

and

$$\frac{1}{D_h} = \frac{1}{D_{1/\nu}} + \frac{1}{D_{\sqrt{\nu}}} + \frac{1}{D_\nu}\,,$$

where

$$D_{1/\nu} = \frac{4}{9\pi}\left(v_d\,\frac{\epsilon}{\epsilon_t}\right)^2\frac{(2\epsilon_h)^{3/2}}{\nu}\,, \qquad D_{\sqrt{\nu}} = \frac{4\sqrt{2}}{9\pi}\left(v_d\,\frac{\epsilon}{\epsilon_t}\right)^2\frac{\nu^{1/2}}{|\Omega_E|^{3/2}}\,,$$

$$D_\nu = \frac{1}{2}\left(\frac{v_d}{\Omega_E}\,\frac{\epsilon}{\epsilon_t}\right)^2\frac{\nu}{\mathcal{F}_{bl}}\,.$$

In these formulae, $\Omega = qB_0/m$ is the gyrofrequency and $\mathcal{F}_{bl} = \sqrt{\epsilon + 2\epsilon_h} - \sqrt{2\epsilon_h}$ is the fraction of pitch-angle space in which toroidally blocked particles exist.

The preceeding expression for D represents an attempt to patch together various results from the analytic theory of neoclassical transport in general toroidal devices, D_t, with those describing the losses due specifically to particles localized in the stellarator's helical ripple, D_h. It must be considered a rough approximation at best, D_t composed of the Pfirsch-Schlüter (D_{PS}), plateau (D_p) and banana (D_b) diffusion coefficients [26,27], and D_h cobbled together from results derived for $\nu_{eff} \gg \Omega_E$ ($D_{1/\nu}$), $\nu_{eff} \lesssim \Omega_E$ ($D_{\sqrt{\nu}}$), and $\nu_{eff} \ll \Omega_E$ (D_ν) [1,4,6,7]. In particular, the usual analytic approximations were demonstrated in figure 1 to be inadequate at the more collisional end of the *lmfp* regime; as a consequence, the analytic theory underestimates D substantially for the range of collision frequencies $1 < \nu_{eff}/\Omega_E < 10$. On the other hand, the analytic expression exhibits reasonably good agreement with the numerical results at smaller values of ν.

A few words must be said regarding the accuracy of the numerical results and the attendant computational times as these two are inextricably linked. This becomes particularly evident deep into the *lmfp* regime and concerns each of the numerical approaches to a various degree.

• For GSRAKE, the number of nodes must be made larger to resolve the increasing localization of the distribution function with decreasing ν. Simultaneously, the value of m_{max} must also increase to provide the coupling to higher-order Fourier harmonics necessary to account accurately for the collisionless variation of the pitch-angle variable. Illustrated quantitatively using the curves plotted in figure 6 as an example, the calculation performed at $\nu_{eff}/\Omega_E = 1$ required $\tau_{CPU} = 0.15$ seconds for $m_{max} = 1$; larger values of m_{max} may be dispensed with as they yield results for D which differ only by tenths of a per cent. At $\nu_{eff}/\Omega_E = 10^{-3}$, however, $m_{max} = 3$ is necessary to achieve a similar coincidence of results and the simulation consumes $\tau_{CPU} = 3.8$ seconds.

• The computational efficiency of FLOCS depends strongly on the mesh configuration which is chosen. Coarser meshes are to be favored over finer — not only do they have fewer mesh points, they also allow larger time steps. The localization of the distribution function observed in the extreme *lmfp* regime is not to be resolved with such meshes, however, and the computational efficiency suffers accordingly. The set of results given here is typical; $\tau_{CPU} = 3450$ seconds — more than 70 per cent of the total computational time — is required for the two most collisionless data points. One final note concerning the FLOCS results: each calculation was initialized with the solution of a neighboring data point and terminated when the computed value of D fluctuated by less than one per cent over a series of consecutive time steps.

• A Monte Carlo simulation consisting of N test particles results in as many discrete values for the monoenergetic diffusion coefficient, designated D_j where j is the particle index. By the definitions of standard statistics these values have a mean and variance of

$$D = \frac{1}{N}\sum_{j=1}^{N} D_j \qquad \text{and} \qquad \sigma^2 = \frac{1}{N-1}\sum_{j=1}^{N}(D_j - D)^2 ,$$

respectively. As the notation suggests, the mean provides a statistical estimate of the monoenergetic diffusion coefficient; the relative error associated with this estimate is given by $\sigma(D\sqrt{N})^{-1}$. An arbitrary level of statistical accuracy is thus theoretically possible if the sample of test particles is made large enough. The practical restriction of finite computer resources is a serious constraint, however, especially deep into the

lmfp regime where the computational time associated with each test particle increases as ν^{-1}. For the Monte Carlo results of figure 6, the relative errors lie in the interval $0.20 > \sigma(D\sqrt{N})^{-1} > 0.05$ and the computational times for a single simulation are as large as 8200 seconds and as little as 40 seconds; the greater value in each case applies to the most collisionless data point while the lesser value is typical of computations at large ν.

• DKES simulations determine upper and lower bounds for the monoenergetic diffusion coefficient; the results given here are the averages of these two values. The degree to which these bounds converge is a strong function of collision frequency, worsening with decreasing ν. This may be amply demonstrated using examples from the data set plotted in figure 6. The calculation at $\nu_{eff}/\Omega_E = 1.6$ was carried out using 55 Fourier modes and 80 Legendre polynomials to describe the solution and consumed $\tau_{CPU} = 2.1$ seconds; the upper and lower bounds are identical to within considerably less than one per cent. At $\nu_{eff}/\Omega_E = 8 \times 10^{-3}$ the upper and lower bounds differ from the average value by twenty per cent in spite of the fact that 325 Fourier modes and 210 Legendre polynomials were employed in the computation, requiring $\tau_{CPU} = 710$ seconds.

A ripple-averaged formalism is physically meaningful only for the description of particles which find themselves in the *lmfp* regime, i.e., particles which satisfy either $\tau_b \nu_{eff} < 1$ or $\tau_t \nu_{eff} < 1$; for the parameters of figure 6, this translates into the requirement $\nu_{eff}/\Omega_E < 10$. In some instances — the current results provide an example — solutions of the ripple-averaged kinetic equation yield reasonably accurate results for D in considerably more collisional cases, as well. Such instances, however, must be considered largely fortuitous; non-localized particles dominate the transport at large ν and their kinetic equations are essentially those of an axisymmetric device, albeit with the "unusual" pitch-angle variable, k^2.

This series of numerical computations has also been carried out for 12 keV electrons and the results are depicted in figure 7. The relative contribution D_t makes to the total monoenergetic diffusion coefficient is greatly reduced for electrons; in the absence of very large electric fields one must therefore expect a significant range of collision frequencies over which $D_{1/\nu}$ scaling will be observed, and this is indeed the case for the present example. It will be noticed that results from the "3-dimensional" codes (Monte Carlo and DKES) lie perceptibly above those of GSRAKE and FLOCS in this $1/\nu$ regime. The discrepancy is largely a consequence of finite ϵ/p effects which are "lost" to the latter codes through ripple averaging; the differences disappear, for example, if the Monte Carlo and DKES simulations are repeated for $p = 60$. The properties of the

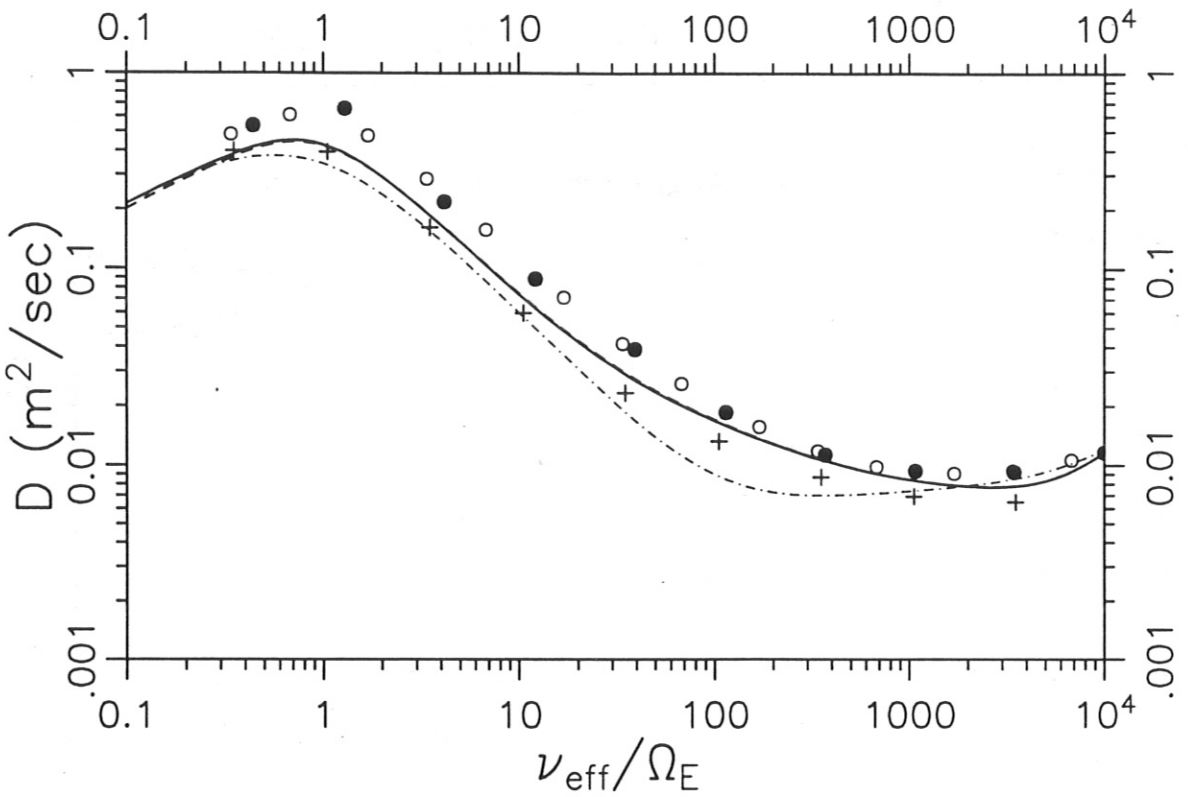

Figure 7. The monoenergetic diffusion coefficient of 12 keV electrons is plotted as a function of normalized collision frequency for an $\ell = 2$, $p = 12$ stellarator with $R_0 = 20$ m, $B_0 = 4$ T, $\epsilon = \epsilon_t = 0.05$, $\epsilon_h = 0.063$, $\iota = 1.47$ and $\Omega_E = 1875$ s^{-1}. GSRAKE results are shown for $m_{max} = 3$ (solid line), $m_{max} = 2$ (dotted line) and $m_{max} = 1$ (dashed line). Each of these curves consists of 100 data points (20 points per decade), requiring total CPU times of 158, 70 and 22 seconds, respectively. Results from FLOCS are shown as crosses (+) $\rightarrow$ 9 data points, total $\tau_{CPU} = 3100$ s. Statistical estimates of D from a guiding-center Monte Carlo simulation are given as solid circles (•) $\rightarrow$ 10 data points, total $\tau_{CPU} = 1.3 \times 10^4$ s. DKES results are plotted as open circles (o) $\rightarrow$ 14 data points, total $\tau_{CPU} = 2370$ s. An analytic approximation for D given in the text is shown by the dot-dash line.

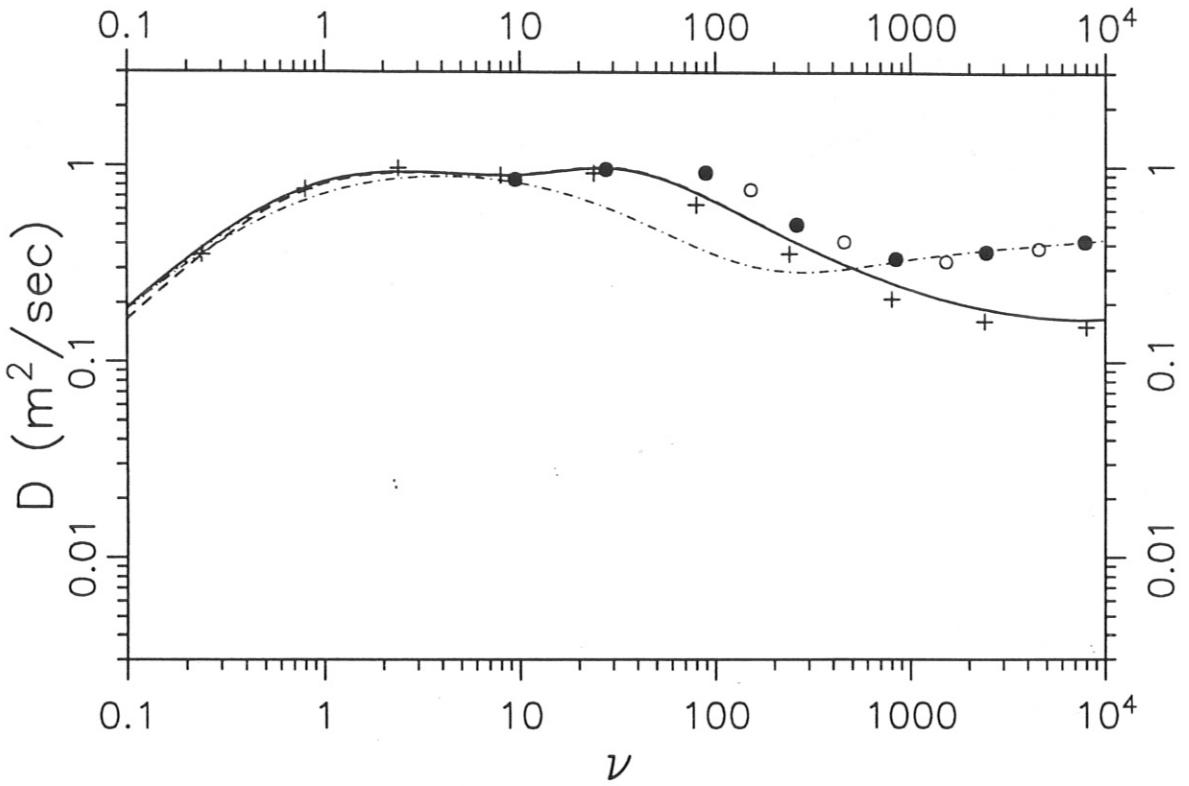

Figure 8. The monoenergetic diffusion coefficient of 12 keV protons is plotted as a function of collision frequency for an $\ell = 2$, $p = 12$ stellarator with $R_0 = 40$ m, $B_0 = 4$ T, $\epsilon = \epsilon_t = 0.025$, $\epsilon_h = 0.063$, $\iota = 1.47$ and $\Omega_E = 0$. GSRAKE results are shown for $m_{max} = 3$ (solid line), $m_{max} = 2$ (dotted line) and $m_{max} = 1$ (dashed line). Each of these curves consists of 100 data points (20 points per decade), requiring total CPU times of 182, 80 and 25 seconds, respectively. Results from FLOCS are shown as crosses (+) $\rightarrow$ 10 data points, total $\tau_{CPU} = 3400$ s. Statistical estimates of D from a guiding-center Monte Carlo simulation are given as solid circles (•) $\rightarrow$ 7 data points, total $\tau_{CPU} = 3070$ s. DKES results are plotted as open circles (○) $\rightarrow$ 4 data points, total $\tau_{CPU} = 8.4$ s (note: for $\Omega_E = 0$, DKES simulations must be confined to the range of collision frequencies $\nu_{eff} > \Omega_h$). An analytic approximation for D given in the text is shown by the dot-dash line.

numerical computations with respect to accuracy and CPU time are very similar to those obtained previously for protons.

Finally, numerical results are presented in figure 8 for a set of simulation parameters which include the assumption $\Omega_E = 0$. In this case only GSRAKE and FLOCS are capable of treating the entire *lmfp* regime — the limitations on DKES in this respect have been stated earlier; the Monte Carlo method fails at low ν because the test particles do not remain sufficiently localized to allow an accurate statistical estimate of D. In the analytic expression for the monoenergetic diffusion coefficient, the helical-ripple contribution is now given by

$$\frac{1}{D_h} = \frac{1}{D_{1/\nu}} + \frac{1}{D_{sp}} + \frac{1}{D_s} ,$$

where

$$D_{sp} = \frac{\sqrt{\pi}}{6} \left(v_d \frac{\epsilon}{\epsilon_t} \right)^2 \frac{\epsilon_h^{1/2}}{|\Omega_h|} , \qquad D_s = 2\sqrt{\pi} \left(\frac{v_d}{\epsilon_t \Omega_h} \right)^2 \epsilon_h \epsilon^{1/2} \nu ,$$

are the expected results in the so-called superbanana-plateau and superbanana regimes, respectively [1,4]. This set of parameters also provides clear confirmation that the use of the ripple-averaged kinetic equation must be confined to the *lmfp* regime ($\nu < 1000$ here); this is always especially evident in stellarator configurations for which the helical ripple is largely responsible for the losses in the plateau regime.

VI. CONCLUDING REMARKS

A general solution of the ripple-averaged kinetic equation has been presented in this paper and used to investigate neoclassical transport in the model magnetic field of a simple stellarator. The solution possesses several desirable traits which are summarized in the following, along with their ramifications.

- The solution is valid throughout the entire *long-mean-free-path* regime and is therefore capable of determining neoclassical transport coefficients for large stellarator experiments and for stellarator reactor plasmas.
- The solution accounts for the entire range of pitch-angle values, treating the regions of velocity space in which *ripple-localized* and *non-localized* particles exist in an equal and self-consistent manner. It has been demonstrated that complete and accurate solutions of the kinetic equations for non-localized particles are indispensable to a comprehensive description of neoclassical transport in stellarators. This refutes the common theoretical approaches in which non-localized particles are ignored entirely or handled in a greatly simplified fashion.

• All drift terms present within the framework of the ripple-averaged theory are accounted for, including the *collisionless* variation of the pitch-angle variable which is routinely neglected in comparison to the *collisional* changes brought about by the Lorentz operator. Further, the poloidal rotation of localized particles includes the full contributions arising due to the $\mathbf{E}\times\mathbf{B}$ and ∇B drifts. The common assumption that the $\mathbf{E}\times\mathbf{B}$ drift dominates may thus be dropped; indeed, the solution may be used to consider cases where precisely the opposite is true.

• The solution has been implemented numerically — in the code GSRAKE — and is extremely efficient computationally. CPU times of a few seconds or less are typical for a single run even for calculations in which the collision frequency is very small. This represents an improvement of more than two orders of magnitude in comparison to previous numerical approaches.

Results obtained with GSRAKE have been thoroughly benchmarked with those of other numerical simulations. A detailed comparison of solutions for the perturbed distribution function has been carried out with GSRAKE's nearest numerical relative, the FLOCS code. Monoenergetic diffusion coefficients for a stellarator reactor plasma have been determined using GSRAKE, FLOCS, a Monte Carlo simulation and the DKES code. Good agreement of the numerical results was observed in all of these comparisons, GSRAKE requiring but a tiny fraction of the computational time necessary for the other calculations.

The computational speed of GSRAKE makes it ideally suited for further studies of neoclassical transport, including a detailed investigation of parameter scalings in the *long-mean-free-path* regime. Future tasks include the extension of the code to treat more general magnetic-field models which accurately describe the majority of stellarator-type devices [25]. Ultimately, this should allow the calculation of neoclassical transport coefficients and self-consistent radial electric fields for such configurations in a fraction of the time usually required.

ACKNOWLEDGEMENT

The authors would like to thank Dr. H. Maaßberg for performing the DKES calculations presented in this paper.

APPENDIX

The conventional analytic theory of neoclassical transport in stellarators makes extensive use of the second adiabatic invariant

$$\mathcal{J} = \oint dl\, m v_{\|} = 2\tau_b \kappa \langle \lambda^2 \rangle_r = \frac{2R}{|\ell_{\mathcal{E}} - p|} \left(\mu B_0 m \epsilon_h\right)^{1/2} A(k^2)\,,$$

which is a constant of the motion for ripple-localized particles. In the set of coordinate variables $(r,\theta,\mathcal{E},\mu)$ the ripple-averaged (or bounce-averaged) drift equations of localized particles may be determined from

$$\langle \dot{r} \rangle_r = \frac{-1}{qrB_0} \left(\frac{\partial \mathcal{J}}{\partial \theta}\right) \left(\frac{\partial \mathcal{J}}{\partial \mathcal{E}}\right)^{-1},$$

$$\langle \dot{\theta} \rangle_r = \frac{1}{qrB_0} \left(\frac{\partial \mathcal{J}}{\partial r}\right) \left(\frac{\partial \mathcal{J}}{\partial \mathcal{E}}\right)^{-1}.$$

Recalling that

$$k^2 = \frac{(\mathcal{E} - q\Phi)/\mu B_0 - 1 + \epsilon_t \cos\theta + \epsilon_h}{2\epsilon_h}$$

and performing the indicated differentiation, one obtains

$$\langle \dot{r} \rangle_r = v_d \sin\theta\,,$$

$$\langle \dot{\theta} \rangle_r = \Omega_E + \Omega_h \langle \cos\eta \rangle_r + \Omega_t \cos\theta\,,$$

where the FLOCS assumptions $\epsilon = \epsilon_t$ and $\kappa \approx \mu B_0$ have been made. Consistent with the usual ordering scheme, $\mathcal{O}(\epsilon_t)$ terms in the drift equations appearing due to the radial and poloidal variation of $R = R_0 + r\cos\theta$ have been neglected.

The invariance of $\mathcal{J}$ may also be used to determine the ripple-averaged expression for the time rate of change of k^2,

$$\frac{d\mathcal{J}}{dt} = 0 = \frac{\partial \mathcal{J}}{\partial r} \langle \dot{r} \rangle_r + \frac{\partial \mathcal{J}}{\partial \theta} \langle \dot{\theta} \rangle_r + \frac{\partial \mathcal{J}}{\partial k^2} \langle \dot{k}^2 \rangle_r\,.$$

Although it is usually thought of as a pitch-angle variable, the calculation here is simplest if k^2 assumes the role of the energy, i.e., if the partial derivatives are taken at constant μ. Before doing so, however, it is important to note that, in general, $r\Omega_E/v_d$ must be considered $\mathcal{O}(\epsilon_t^{-1})$, with the consequence that $(\partial \mathcal{J}/\partial\theta)\langle\dot{\theta}\rangle_r$ is $\mathcal{O}(1)$ and may not be neglected. (This fact was overlooked in previous derivations [19,20] which assumed $R = R_0$ at the outset.) It is then straightforward to show that

$$\langle \dot{k}^2 \rangle_r = \left(\epsilon_t \Omega_E - \frac{\epsilon_t}{2\epsilon_h} \Omega_h \right) \sin\theta \, \frac{A(k^2)}{A'(k^2)} \,,$$

where, once again, $\mathcal{O}(\epsilon_t)$ corrections to this expression have been dropped.

Implementation of the numerical scheme employed in the FLOCS code is greatly facilitated by expressing the kinetic equation in conservation form, stipulating that the phase-space flow be divergence free

$$\frac{1}{J_r} \left(\frac{\partial}{\partial r} \left(J_r \langle \dot{r} \rangle_r \right) + \frac{\partial}{\partial \theta} \left(J_r \langle \dot{\theta} \rangle_r \right) + \frac{\partial}{\partial k^2} \left(J_r \langle \dot{k}^2 \rangle_r \right) \right) = 0 \,,$$

where

$$J_r \approx 4\pi r R \left(\frac{\kappa \epsilon_h}{m^3} \right)^{1/2} A'(k^2)$$

is the ripple-averaged Jacobian. It may be readily verified that this "three-dimensional" condition is satisfied in leading order, but this proves to be insufficient in two respects. First, to be numerically useful the divergence must be exactly zero, and second, the ordering of the kinetic equation eliminates r as a variable from the problem (leaving it the status of a mere parameter), forcing the divergence condition to be satisfied in the remaining two dimensions (θ,k^2). These two requirements are most easily met by setting $R = R_0$ in the Jacobian and by replacing the true expression for the poloidal drift frequency with one including small "fictitious" terms

$$\langle \dot{\theta} \rangle_r = \Omega_E \left(1 + \epsilon_t \cos\theta \right) + \Omega_h \left(\langle \cos\eta \rangle_r - \frac{\epsilon_t}{2\epsilon_h} \cos\theta \right) .$$

If it is further assumed that $\partial \epsilon_h / \partial r = 2\epsilon_h / r$ one may substitute $\Omega_h(\epsilon_t / 2\epsilon_h) = \Omega_t$, which is the expression used in the FLOCS code. For cases of interest, the fictitious terms represent $\mathcal{O}(\epsilon_t)$ changes in $\langle \dot{\theta} \rangle_r$ and thus do not violate the ordering scheme. This need not be true, however, when more complicated model magnetic fields are treated [28]; careful interpretation of the results may be necessary in such cases [29].

REFERENCES

[1] Galeev A A, Sagdeev R Z, Furth H P and Rosenbluth M N, 1969 **Phys. Rev. Lett. 22**, 511

[2] Kovrizhnykh L M, 1969 **Sov. Phys. JETP 29**, 475

[3] Kadomtsev B.B. and Pogutse O.P., 1971 **Nucl. Fusion 11**, 67

[4] Galeev A A and Sagdeev R Z, 1979 **Reviews of Plasma Physics, Vol. 7, Leontovich M A, Editor**, (Consultants Bureau, New York) p 257

[5] Wakatani M, 1983 **Nucl. Fusion 23**, 817

[6] Mynick H E, 1983 **Phys. Fluids 26**, 2609

[7] Shaing K C, Rome J A and Fowler R H, 1984 **Phys. Fluids 27**, 1

[8] Kovrizhnykh L M, 1984 **Nucl. Fusion 24**, 851

[9] Ho D D-M and Kulsrud R M, 1987 **Phys. Fluids 30**, 442

[10] Beidler C D, Hitchon W N G, van Rij W I, Hirshman S P and Shohet J L, 1987 **Phys. Rev. Lett. 58**, 1745

[11] Gott Yu V, 1989 **Sov. J. Plasma Phys. 15**, 822

[12] Kovrizhnykh L M and Shasharina S G, 1990 **Nucl. Fusion 30**, 453

[13] Potok R E, Politzer P A and Lidsky L M, 1980 **Phys. Rev. Lett. 45**, 1328

[14] Boozer A H and Kuo-Petravic G, 1981 **Phys. Fluids 24**, 851

[15] Wobig H, 1982 **Z. Naturforsch. 37a**, 906

[16] Dommaschk W, Lotz W and Nührenberg J, 1984 **Nucl. Fusion 24**, 794

[17] Fowler R H, Rome J A and Lyon J F, 1985 **Phys. Fluids 28**, 338

[18] Beidler C D, Hitchon W N G and Shohet J L, 1987 **J. Comput. Phys. 72**, 220

[19] Mynick H E and Hitchon W N G, 1986 **Nucl. Fusion 26**, 425

[20] D'haeseleer W D, Hitchon W N G and Shohet J L, 1991 **J. Comput. Phys. 95**, 117

[21] Hirshman S P, Shaing K C, van Rij W I, Beasley C O Jr. and Crume E C Jr., 1986 **Phys. Fluids 29**, 2951

[22] van Rij W I and Hirshman S P, 1989 **Phys. Fluids B 1**, 563

[23] D'haeseleer W D, Hitchon W N G, Beidler C D and Shohet J L, 1990 **J. Plasma Physics 44**, 431

[24] Miyamoto K, 1974 **Phys. Fluids 17**, 1476

[25] Beidler C D and Hitchon W N G, 1994 **Plasma Phys. Control. Fusion 36**, 317

[26] Boozer A H, 1981 **Phys. Fluids 24**, 1999

[27] Rodriguez-Solano Ribeiro E and Shaing K C, 1987 **Phys. Fluids 30**, 462

[28] Hitchon W N G and Mynick H E, 1987 **J. Plasma Physics 37**, 383

[29] Beidler C D, 1987 **Univ. Wisconsin Report TSL-87-7**